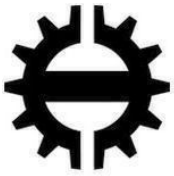

TAMPERE UNIVERSITY OF TECHNOLOGY
Master's Degree Programme
in Biomedical Engineering

ZAIDA CEBRIAN JIMENEZ

SIMULATIONS OF THE ELECTRICAL ACTIVITY OF CARDIOMYOCYTES DERIVED FROM HUMAN EMBRIONIC STEM CELLS

Master of Science Thesis

Examiners: Jari Hyttinen
Juho Väisänen
Examiner and topic approved in the Science and Environment Faculty Council meeting on 3rd September 2008

ABSTRACT

TAMPERE UNIVERSITY OF TECHNOLOGY
Master's Degree Programme in Biomedical Engineering
CEBRIAN JIMENEZ, ZAIDA: Simulations of the electrical activity of cardiomyocytes derived from human embryonic stem cells
Master of Science Thesis, 64 pages, 11 Appendix pages
January 2012
Major: Medical Instrumentation
Examiner: Professor Jari Hyttinen, PhD Juho Väisänen
Keywords: cardiac modelling, lead fields, cardiomyocyte, stem cells

In this thesis, a cellular automata based modelling software is developed for studying the electrical activation of cardiomyocytes. The mathematical models help to simulate and study different phenomena related to the cardiac activation. They enable flexible studies for healthy and unhealthy tissue and give a better understanding of the behaviour of the electrical propagation in the heart. The models which are implemented with a graphical user interface are easier to use for inexpert users. This makes these programs very helpful for educational purpose as well as valuable tools for research groups.

Nowadays, one of the aspects of the research in the cardiac field is the stem cells. Cardiomyocytes derived from stem cells are being grown in the laboratories to be analysed and used in drug screening. The differentiation of the cells in a particular type is not straightforward. There can be several types of cardiac cells (ventricular, atrial or sinoatrial myocytes) in the same cell culture. Patch clamp is used to discern which types of cells were grown and microelectrodes arrays (MEA) are used to measure the electrical signals produced by the cultures. Patch clamp is costly and time consuming process to identify the cells.

The main goal of this master thesis is to study the differences in the simulated electrograms (EGM) from the normal electrodes recordings when the type of cell is changed. If there are quantitative changes the EGM, it could be possible to know a priori which type of cardiomyocyte is present in the culture without having a patch clamp study.

The model simulates the electrical activity of cell culture with a cellular automaton based on cardiomyocyte action potential and the conduction velocity curves. These curves are known as restitution curves of the cardiac tissue. It is also needed to model the geometry of the cell culture and the MEA electrodes. This geometry and its lead fields calculated with a finite difference model (FDM) are the inputs for the cellular automata.

The cellular automata and the FDM model of the cell culture were successfully performed. The results show that there are differences in the EGM when the action potential of each type of cell is set in the model. The biggest difference is between the contractile cells and the pacemaker ones. The cells could be classified a priori with this study, but in the real life there are more factors that are included and not just one type of cell. There is a need to try in vitro models to check this hypothesis.

PREFACE

This thesis was done in the Department of Biomedical Engineering of Tampere University of Technology. The biological data was provided by Regea Institute for Regenerative Medicine, a joint institute under the administration of the University of Tampere.

I would like to thank my supervisors Jari Hyttinen and Juho Väisänen for the guidance during the development of this thesis. They have introduced me to the world of modelling and they have helped during my stay in Finland. I also want to thank Katriina Aalto-Setälä, Erja Kerkelä and Ville Kujala for their help in all the biological aspects of this thesis. I would like to thank Jesus Requena who introduced me to the cardiology world and brought me to Finland.

I would also like to thank my family and my friends who have given me support in all the difficult moments during these years. They have made my life in Finland easier and they have always pushed me to carry on. I want to have a special mention to Amelia, Amparo, Saul and Mamen who were there for me in my first days at Finland. And I cannot forget Paula and Nazia with whom I have shared so many good moments. Thank you.

Zaida Cebrián Jiménez

Table of Contents

Abbreviations and acronyms

antSC	Altered nuclear transfer derived stem cells
APD	Action potential duration
AV node	Atrioventricular node
BEM	Boundary element method
CV	Conduction velocity
ESC	Embryonic stem cells
ECG	Electrocardiogram
EGM	Electrogram
FDM	Finite difference method
FEM	Finite element method
iPS	Induced pluripotent stem cells
MEA	Microelectrode array
ntSC	Nuclear transfer stem cells
SA node	Sinoatrial node

1 Introduction

The adult heart lacks of effective mechanisms for healing ischemia or infarction. Stem cells are being studied in this aspect. There are some experiments that show the benefits the implantation of new cardiomyocytes derived from stem cells into the heart (1). Drug screening is the other big application of stem cells in this field. Thanks to the advances in the regenerative medicine, now it is possible to convert patients own adult cells such as skin cells into stem cells (2) (3). Therefore, it is possible to have stem cells from each specific patient to perform drug screening.

The stem cells are cultured *in vitro* and then they are differentiated into cardiomyocytes. One of the problems during this process is how to determine which types of cardiomyocytes are been derived (atrial, ventricular or sinoatrial cells). The only way to be certain about the nature of the cells is the patch clamp. This is a technique which measures the voltage across the membrane for a specific cell (4). But this method implies that all the cells should be analysed to be able to confirm that they are from a specific type of cardiomyocytes. This is the main motivation for this project, to be able to find which type of cells are been recorded by a MEA without the need of prior knowledge from the patch clamp.

In this thesis, a cellular automata model for cardiomyocytes is developed to study the differences in the simulated electrograms (EGM) from multielectrode array (MEA) when different action potentials are used. It is needed to have a computer model with known types of cardiomyocytes, as the cell cultures will have unknown types of cardiomyocytes. There are models that simulate the ionic currents through the membrane (cell models). These models simulate the voltage across the membrane (5) (6) (7) (8). There are other models that describe the propagation of the signals in a region as a whole without taking into account the detail level of each specific cell. This second type of models is the appropriate one for this thesis because the MEA electrodes record the electrical activity of the cells as a whole not cell by cell. There are several types of electrical conduction models: simplified models (9) (10), reaction diffusion models and cellular automata (11) (12) (13), which will be reviewed in this thesis. The cellular automaton is the model chosen in this work because its computational load is smaller than in the other cases.

In this work, the complete process of modeling of a cell culture is shown. The cellular automaton is developed and explained. The geometry model of the cell culture and its finite difference model (FDM) are calculated to find the lead fields. Before trying to proof the hypothesis, there is a study of the lead field behavior and test of the functionality of the automaton under known conditions.

2 Background

2.1 Physiology

This chapter explains the physiological background that is needed for this thesis. First, a presentation of the heart physiology and the electrical activation in the heart is made. Some small introduction of the stem cells will be given as well as the electrical behaviour of the cardiomyocytes.

2.1.1 Heart

The heart is the essential organ of the cardio vascular system. It is a striated muscle that absorbs the blood from the veins and expels it through the arteries. The striated muscle is called myocardium and it is covered by the pericardium at the outside and by the endocardium at the inside. The heart is located in the thorax between the lungs and behind the sternum.

The heart is divided in four chambers, two superior ones (atria) and two inferior ones (ventricles), and they are separated by heart valves which allow blood to flow in only one direction through the heart chambers, from the atria through the ventricles and from the ventricles to the arteries leaving the heart. (4).

The heart behaves as a double pump system. The right side works as the pulmonary circuit pump while the left side works as the systemic circuit pump. The pulmonary circulation is the one that comes from the right side of the heart to the lungs and back to the left side of the heart. The systemic circulation will take the blood from this left atrium and pump it out from the left ventricle into the aorta artery. This blood is supplied to all the organs in the body which will take the oxygen and nutrients. The non-oxygenated blood is taken back to the right atrium through the veins. Because the left ventricle is the systemic pump that pumps blood over a much longer pathway through the body, its walls are substantially thicker than those of the right ventricle, and it is a much more powerful pump (14).

The structure of the heart is presented in Figure 2.1.

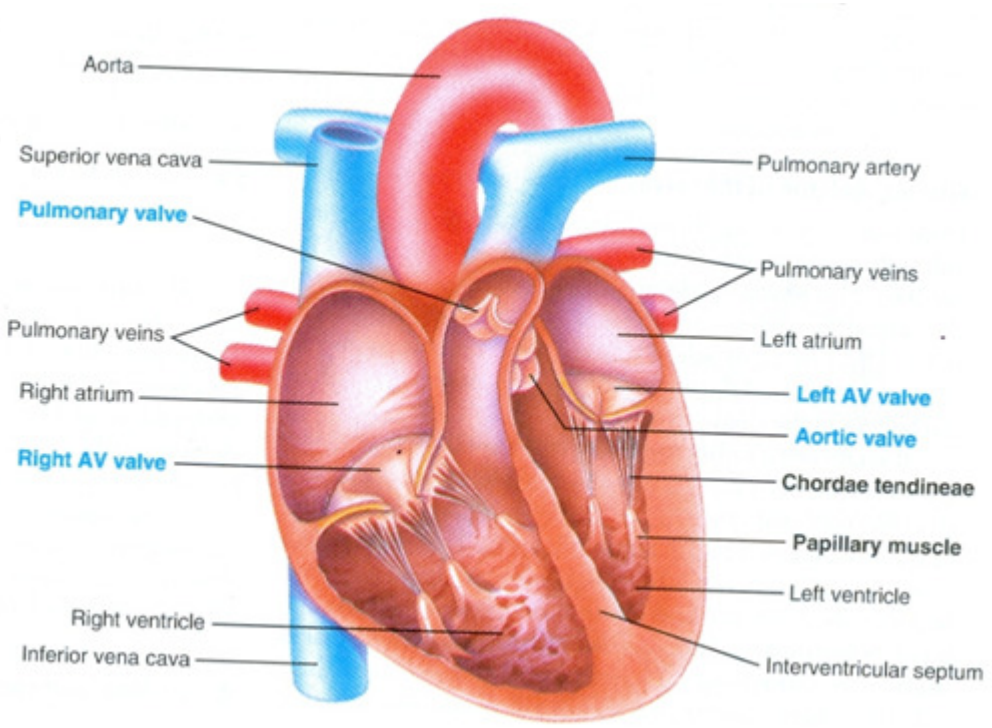

Figure 2.1. Structure of the heart (15)

2.1.2 Electrical activity in the heart

The heart is composed of cardiac muscle cells that generate and/or conduct action potentials created when there are the ion currents across the cell membrane. These action potentials are propagated through the heart in the direction of the muscle and make it contracts.

The most of the cardiac muscle cells are contractile cells that do mechanical work to pump the blood. These cells are the cardiomyocytes. They are connected between each other through intercalated discs. These discs are form by desmosomes and gap junctions. The desmosomes are adhering junctions which holds the cells together and they exists in tissues with considerable mechanical stress. The gap junctions are areas of low electrical resistances between cells that allow the propagation of the electrical impulses among the cells. Thanks to this mechanism the cells will propagate the electrical impulse to the surrounding cells in a way that they will contract as a single forming what is called the functional syncytium. (15)

Some of the cardiac muscle cells within the heart do not just propagate the electrical impulses, but they generate them. These cells show a pacemaker activity. They don't have a resting potential. Instead, their membrane potential slowly depolarizes between

action potentials until a threshold is reached. At this moment the membrane fires the action potential. This slow drift until the threshold is called the pacemaker potential. (15)

These cells which show a pacemaker activity are distributed in specific parts of the heart:

1. The sinoatrial node (SA node) is in the superior part of the right atria and it is where the normal heart beat is initiated. The pulse frequency is around 70 beats per minute.
2. The atrioventricular node (AV node) is situated at the base of the right atrium and it is the only electrical connection between the atria and the ventricles. Its pulse frequency is around 40 beats per minute.
3. The bundle of His starts in the AV node and divides into left and right ventricle. The small terminations of the bundle of His are called Purkinje fibres and they spread throughout all the ventricular myocardium. The pulse frequency of these fibres is around 20 beats per minute. (15)

In the normal situation the SA node generates the action potential (because it has the bigger potential rate) and it propagates it to the left atria through the interatrial pathway. Therefore, both atria will contract at the same time. The electrical impulse reaches the AV node and it is delayed about 100ms so that the atrium and ventricles will not contract at the same time. Then the electrical activity is propagated to the ventricles through the bundle of His and the Purkinje fibres which propagate the electrical activity faster (Figure 2.2 and 2.3). Within 30 milliseconds the action potential has been propagated to the entire ventricles which will contract as a unit. (15)

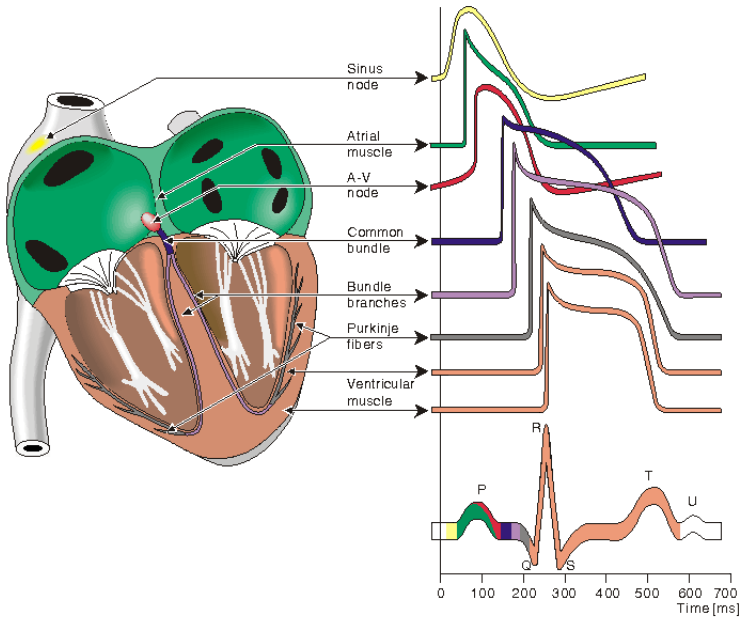

Figure 2.2 Activation and propagation of the electrical activity in the heart. (4)

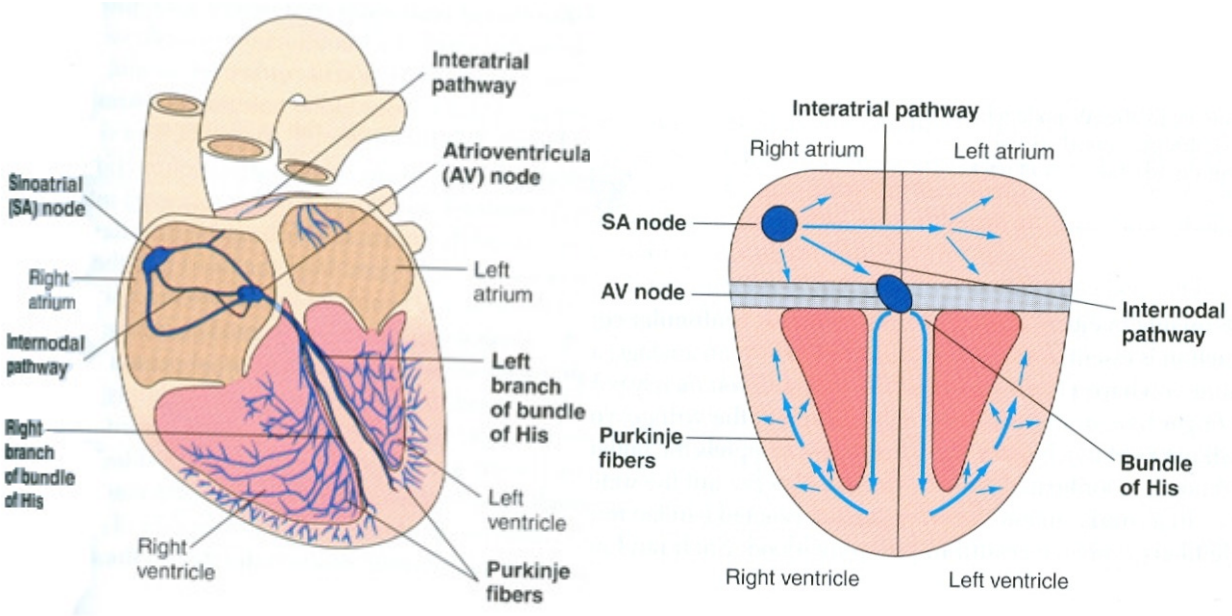

Figure 2.3. Specialized conduction system of the heart. Spread system of cardiac excitation (15)

When there are heart disease and blocking in the conduction channels, the other pacemakers takes the function of generating the action potentials but at slower rates. These can be observed in the changes in the form of the electrocardiogram (ECG). (4)

ACTION POTENTIAL FROM THE PACEMAKER CELLS

The pacemaker potential is generated due to the closure of the K^+ channels and the constant inward Na^+ current, because this type of cells don't have voltage-gate Na^+ channels (Figure 2.4). Before the threshold is reached the transient Ca^{2+} channels, which are voltage dependent are open, depolarizing further the membrane. When the threshold is reached, the longer-lasting voltage gated Ca^{2+} channels are opened creating the rising phase. The falling phase is due to the overture of the voltage-gated K^+ channels. (15)

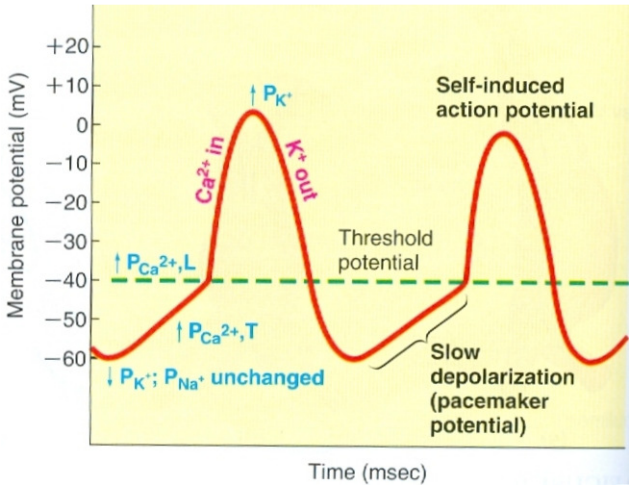

Figure 2.4. Pacemaker activity of cardiac autorhythmic cells, showing the different flow of ions in each phase. (15)

The different pacing rates come from the faster or slower rate of depolarization. As we can see in figure 2.5, the cell with slower rate of depolarization will trigger the action potential later and therefore will never set the pacing rate of the heart if there is a faster one.

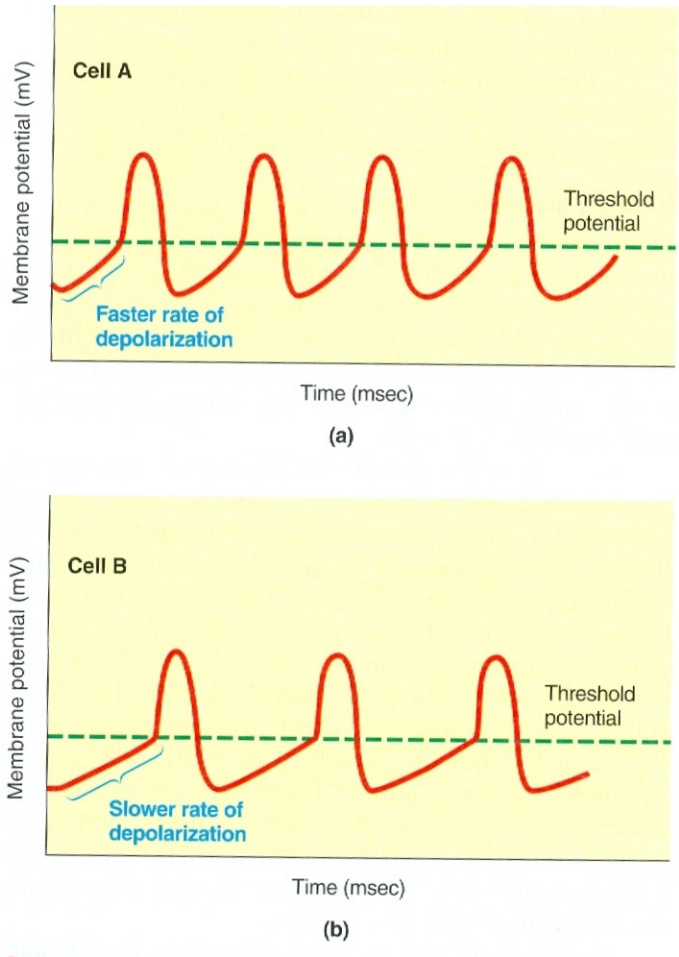

Figure 2.5. Different autorhythmic rates for two pacemaker cells. When having both cells in the same tissue, it will only propagate the electrical activity from the cell with faster rate of depolarization. (15)

ACTION POTENTIAL FROM THE CARDIOMYOCYTES

The action potential of the cardiomyocytes differs from the pacemaker cells as it can be seen in Figure 2.6. In this case the cells are at -90 mV in the resting state. When the action potential of the pacemaker cells reaches the cardiomyocyte, the cell membrane becomes more permeable to Na+ and the rapid increase of Na+ raises the voltage to 30mV. Then the permeability to Na+ is reduced, but the membrane potential is maintained for several hundred of milliseconds due to the slow Ca2+ current producing the plateau phase. This plateau phase is a typical characteristic of the cardiac cells. When the Ca2+ channels are closed, the K+ channels become more active producing the rapid repolarization of the cell. (15)

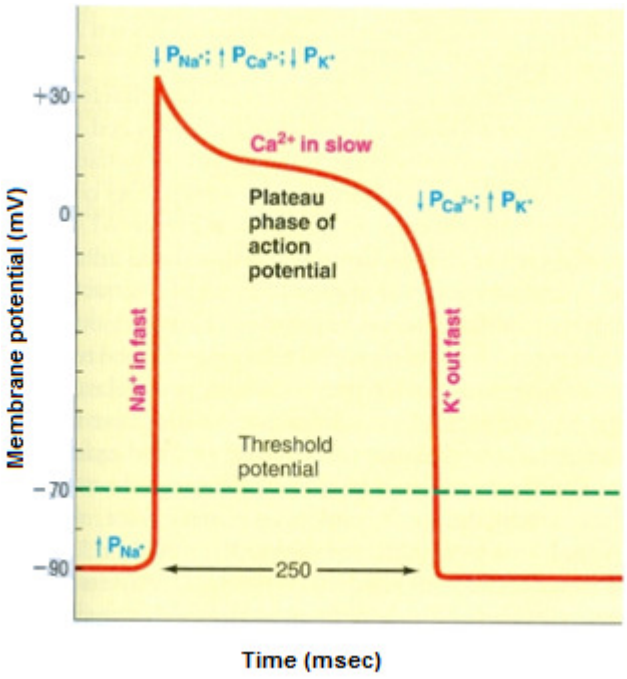

Figure2.6. Action potential in ventricle myocyte, showing the different flow of ions in each phase. (15)

The action potential of the ventricular and atrial cells is very similar but atrial cells have almost no plateau phase due to a smaller calcium influx. This effect can be seen in Figure 2.7.

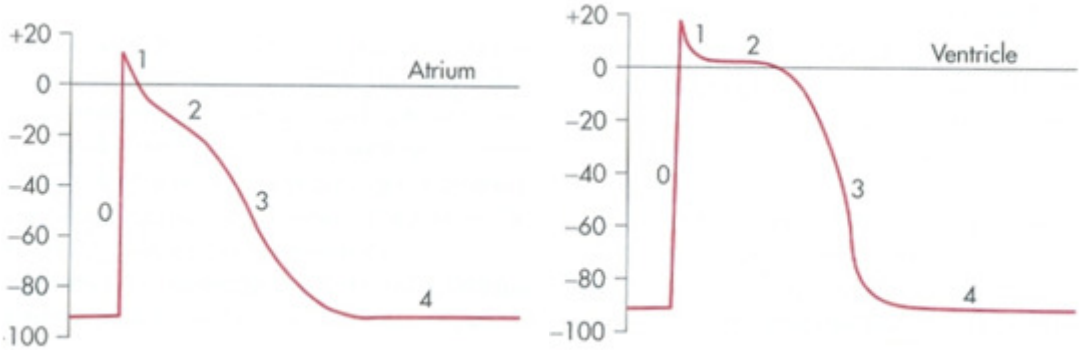

Figure2.7. Action potential of an atrial myocyte and a ventricular myocytes. In atrial myocytes the plateau phase (phase 2) is not as flat as in ventricular myocytes. (16)

RESTITUTION CURVES

The restitution curves are a way to show how the cells adapt to changes in the beating rate. The curves show the relationship between the duration of the action potential (action potential duration APD) and the interval of time preceding it (diastolic interval DI) and between the conduction velocity (CV) of the action potentials and the diastolic interval.

The action potential duration curve is generated by pacing the cells in specific moments producing different diastolic intervals and measuring the duration of the action potential. Normally the duration of the action potential is calculated as the time between the upstroke and the moment when the repolarization has reach the 90% of the total value.

The measurement of the conduction velocity is more difficult due to the anisotropy of the tissue. The propagation is not the same in every direction and the fibres can change their orientation. The velocity is measured between two points and therefore is the average of the conduction velocity of the cells in that area.

Some typical curves for the cardiac tissue are shown in Figure 2.8. When the beating rate increases, the diastolic interval is smaller and the action potential gets shortened.

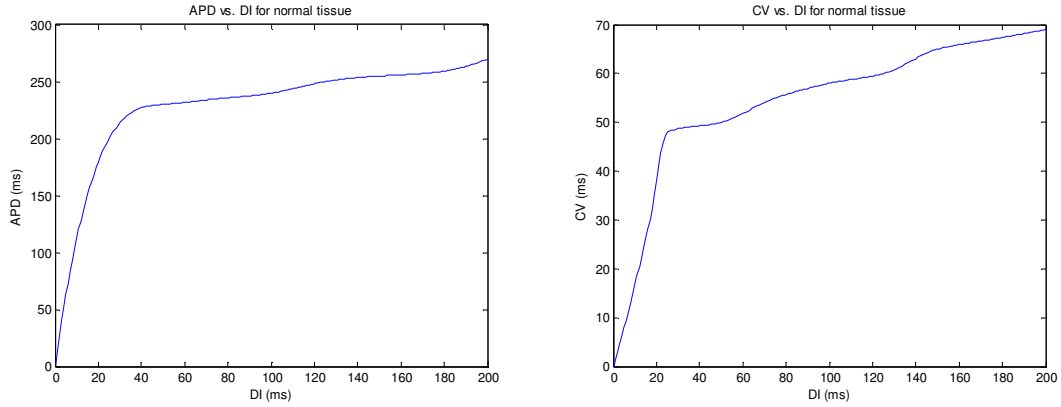

Figure 2.8. Restitution curves for a healthy tissue: a) APD restitution curve; b) CV restitution curve. (17)

2.1.3 Methods to measure the membrane currents

There are several methods to study the electrophysiology of the cells. Voltage clamp was the first method to measure the currents across the cell membrane but the patch clamp method has become more common nowadays, used as a whole cell clamp (18). A new method to study the electrophysiological properties of cell populations have been developed with the help of MEA (19).

VOLTAGE CLAMP

The method was first developed by Cole (1949) (20) and Hodgkin et al (1952) (21). It was thought to be used with the squid giant axon but the method has evolved to be used in many types of tissues.

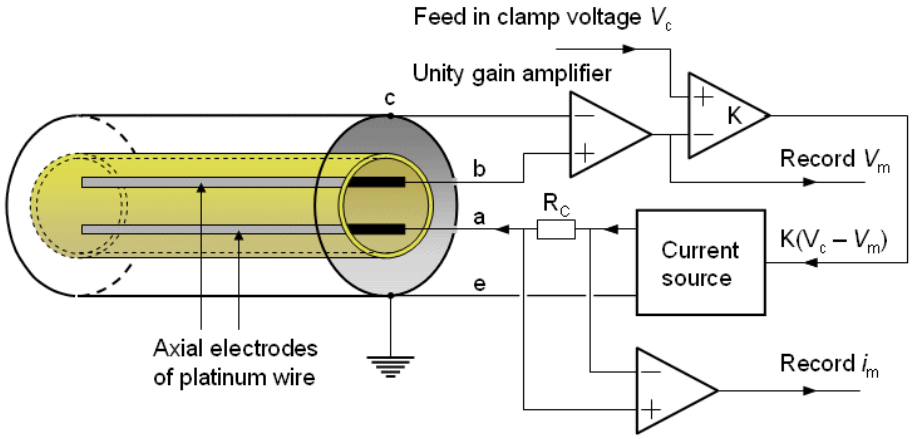

Figure 2.9. Schematic diagram of the electric configuration of the voltage clamp. (4)

The voltage clamp is used to measure the ion currents across the membrane while setting the membrane voltage at a certain level. It studies the relationship of the current and the voltage across the membrane. The user sets a certain level while the membrane voltage is being measure by an electrode. These two voltages are connected to an amplifier which obtains the difference between both signals (Figure 2.9). This difference is compensated injecting a current to the cell until the difference is zero. Every time that there is a deviation from the membrane voltage with respect to the voltage level, a current is injected to the cell. This current has the same value but with a different sign as the ionic currents through the membrane. Thus, recording this current, the ionic currents are recorded. (18)

PATCH CLAMP

The patch clamp technique is a method to measure the current from single or multiple channels in excised membrane patches. It was first used by Neher and Sakmann in 1976 (22) and latter developed by them in 1978 (23) and by Hamill et al in 1981 (24). It is a method with higher resolution than voltage clamp and it can also be used with very small cells and cells which are not electrically excitable. (18)

Instead of using electrodes which penetrate the cell membrane, patch clamp uses a glass micropipette with an opening in the tip. This type of electrodes seals to the surface of the cell when suction is applied. It is filled with a solution which matches the ionic composition of the bath solution in cases of cell attached recordings or the ionic composition of the cytoplasm in the case of the whole-cell recording. (18)

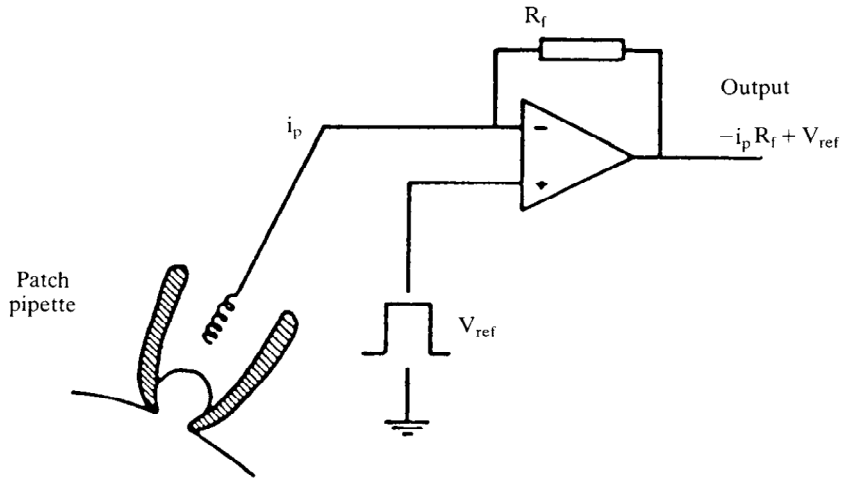

Figure 2.10. Schematic diagram of the electric configuration of the patch clamp. (18)

The recordings are made using an electrode inside the glass micropipette and an amplifier as show in Figure 2.10. The reference voltage is set to the voltage recorded by the electrode when the micropipette is not in the cell, obtaining a zero voltage at the output. When the seal is obtained, the membrane currents are recorded by the electrode and show at the output as a difference with respect to the reference voltage. (18)

When the seal is done, the electrical isolation of the cell membrane patch is better and the noise is reduced. This is a very important advantage which makes it possible to perfume high resolution recordings. (18)

MICROELECTRODES ARRAY

MEA is a device with several electrodes which can record the electrophysiological activity of excitable cells and tissues in all the electrodes simultaneously. These arrays can be used in vivo (implantable MEAs) or in vitro (non-implantable MEAs).

In 1972, Thomas et al. used a MEA in their experiments to record the electrical activity form a cell culture for the first time (25). Five years later, without having notice of this work, Gross et al. show their work with MEAs in a snail ganglion (26). The size of the electrodes in both cases were between 7-10 µm with a distance between electrodes of hundreds micrometers. These studies were complicated because the MEA had to be custom made in the laboratories. Nowadays, there are several commercial MEAs available in the market and their use in the laboratory experiments is increasing. There are several experiments which use MEA systems to study cardiomyocytes from various origins, such as the chick heart (27), mouse embryonic stem cell (ESC) derived cardiomyocytes (28), mouse induced pluripotent stem (iPS) cell derived cardiomyocytes

(29), human ESC derived cardiomyocytes (30) (31) and human iPS cell derived cardiomyocytes (32) .

The advantages of this system over the methods described before are the possibility to place several electrodes at once instead of doing it individually, the ability to record simultaneously date from multiple sites of the cell culture or the possibility to select different areas of recording within the array. But the biggest advantage with respect to patch clamp is that MEA systems are non-invasive and they don't need to penetrate the cell membrane.

2.1.4 Stem cells

Stem cells are unspecialized cells that have the potential to continuously self-renew through cell division. Another characteristic of stem cells is that they can be induced to develop into specialized cells, such as cardiomyocytes, in suitable physiological and experimental conditions. (33) Stem cells discovery is not a recent issue. The first bone marrow transplantation was performed already in 1968 at the University of Minnesota, U.S.A. Thereafter, the first embryonic stem cell (ESC) lines were generated in 1981 from mouse blastocysts and in 1998 the first human ESC line was established. (34). The latest studies show the possibility to induce plurpotency in adult stem cells, known as induced pluripotent stem cells (iPS). (2) (3)

Although there are many types of stem cells, they are often roughly categorized into adult stem cells and embryonic stem cells. Naturally, different stem cells have different properties. Perhaps the most important difference relates to the potency of stem cells, in other words, the ability of stem cells to induce other kinds of cells in the body. Stem cells can therefore also be categorized into totipotent, pluripotent, multipotent and unipotent stem cells. Totipotent stem cells are able to differentiate into any kind of human cell. The only totipotent cell is the zygote which can create a whole living being as well as the placenta to support it during the pregnancy. Pluripotent stem cells, on the other hand, are derived from totipotent stem cells and they possess almost the same qualities as these, but they cannot create the placenta. An example of them is the cells of the inner mass of the blastocyst. Multipotent stem cells descend from pluripotent stem cells and they can differentiate into many cell lines within a certain tissue as most of the adult stem cells. Finally, unipotent cells descend from multipotent cells and they have the ability to induce only one cell type.

Adult stem cells can also be referred to as tissue stem cells or somatic stem cells. Adult stem cells are undifferentiated cells derived from adult tissue and they can usually give rise only to the specific tissue cells of the tissue that they were extracted from. The adult stem cells are found in small quantity in small niches in the human body. As they are difficult to discern, it was thought that not all the tissue had them and it was just places as the bone marrow where they could be found. Latest discoveries have found adult stem cells also in maurine pancreas (35) and heart (36) (37) among others. Adult stem cells can be considered to have four major sources cell progenitors: the ectoderm, mesoderm and endoderm as well as the umbilical cord which are shown in Table 2.1. Benefits of the use of adult stem cells include the exclusion of ethical issues related to the use of embryonic stem cells. However, adult stem cells are more likely to contain genetic abnormalities (34). They are difficult to harvest and the proliferation rate is also small (38). For this reason, many of the studies in stem cells are carried out with embryonic stem cells.

Table 2.1. *The progenitors of adult stem cells* (34)

ADULT STEM CELL	Ectoderm	Neural stem cells Ocular stem cells Skin stem cells
	Mesoderm	Hematopoietic stem cells Bone marrow stem cells Stromal stem cells Cardiac stem cells
	Endoderm	Pancreatic stem cells Ovarian and testicular stem cells Gastrointestinal tract stem cells Pulmonary epithelial stem cells Hepatic oval stem cells Mammary and prostatic gland stem cells
	Umbilical cord	Mesenchymal stem cells Hematopoietic stem cells

Embryonic stem cells are obtained from the inner cell mass of a blastocyst, which is an early embryo a few days of age. Embryonic stem cells have been shown to be pluripotent. That is, they are able to form almost all human cells, except those related to fetal development such as placental cells, umbilical cord cells and amniotic cells. (34)

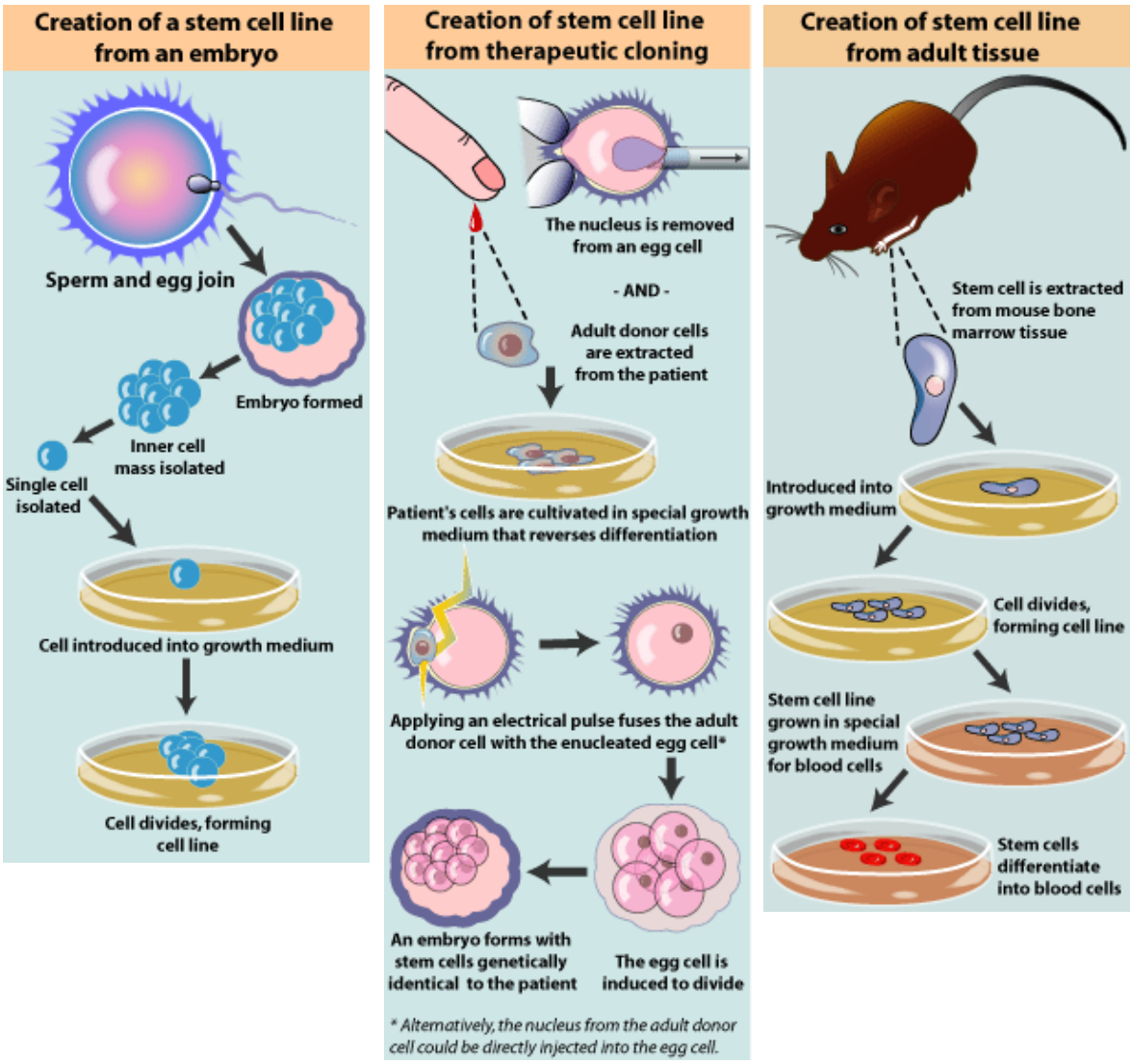

Figure2.11. Different methods to obtain a stem cell line. a) Stem cell line obtained from an embryo; b) Stem cell line obtained from nuclear transfer; c) Stem cell line obtained from an adult tissue (39)

There are several ways to produce embryonic stem cells and each of them has different medical and ethical problems:

- Embryonic stem cells (ESC): The cells are obtained from the inner cell mass of a five days old embryo. The medical concern related with this type of stem cells is the rejection when implanted in the receptor. As the stem cells are genetically different from the receptor, there is a possibility that the body will take them as an external body to be eliminated. The major ethical problem is the destruction of the embryo. The embryo is obtained in a laboratory using the in vitro fecundation method and it could create a new person when implanted in a woman's uterus.(Figure 2.11)

- Nuclear transfer stem cells (ntSC): To obtain this type of stem cells, a genetic code of a normal cell (skin, heart…) is introduced in the nucleus of an enucleated unfertilized oocyte. This oocyte is induced to divide forming an embryo with the same genetic code as the patient. This method avoids the problem with the compatibility with the patient. In the other hand, it has the same ethical problems as before because the embryo can still be implanted in a woman's uterus (Figure 2.11).

- Altered nuclear transfer derived stem cells (antSC): This method is similar to the previous one but one of the genes is altered. This alteration makes the embryo not feasible to be implanted because it cannot create a placenta. This would remove some of the ethical problems and it would not have the rejection problem. But it raises a new issue that is how this alteration in the genetic code can create alterations in the cellular system.

- Induced pluripotent stem cells (iPS): This method was discovered in 2006 by Takahashi. An adult cell is injected with a retrovirus that produces an alteration in the genes of the cell. The alteration is done in markers Oct4, Sox2, c-Myc, and Klf4 (38). This change in the genes creates the pluripotency of the cell. With this method, there is no need of an embryo and there is no rejection in the patient. The main problem is the use of a virus to change the markers which can contaminate the samples.

When the stem cells are collected, they are maintained in a certain culture conditions to keep them undifferentiated. They are cultured over mouse feeder cells to give them the nutrients and molecules that prevent differentiation. When there is a need to differentiate the cells, the cells are placed in a new culture medium with the differentiation and growing factors needed to become that specific type of cells. One of the problems in the differentiation process is that not all the cells mature at the same rhythm and the culture will have cells of different stages of maturity. There also the problem of not having homogeneous cell cultures with just one type of cells but having different types and even some undifferentiated cells still. These problems have to be overcome to be able to use the cell cultures in the treatment with human beings. (40) (41)

2.2 Modelling of the Heart

Now that the physiology had been explained, it is needed to explain how to model all of this. First, we are going to explain how the heart can be modelled. Afterwards, we will talk about the modelling of the electrical signal that the heart generates. It should be notice that this thesis only deals with electrical activity of the heart. This is the reason why there will be no explanation about the mechanical modelling of the heart.

When we are talking about modelling of the electrical activity in the heart, we can look at this activity in different levels: the microscopic level (cellular level) or the macroscopic level (tissue level or whole heart). Both levels would be explained in this section.

2.2.1 Modelling of the cells

The modelling of cells describes how the ionic currents in the membrane of the cell generate the action potential. The ionic currents are produced by the movement of the ions across the membrane through the ion channels. Each channel is sensitive to a specific type of ion. The most important ones are Na^+, K^+, Ca^{2+}, and Cl^-. The opening and closing of the channels depends on several factors and there are different channels with different behaviour for a specific ion.

Most of these transmembrane currents are based on diffusion. The difference of voltage between the membrane and the Nernst potential makes the ion flow inside or outside the cell. This current is described as:

$$I_Y = g_Y(V - E_Y)$$

where g_Y is a conductance term, V is the membrane potential or voltage, and E_Y is the Nernst potential for ion species Y. The Nernst potential is calculated as:

$$E_Y = \frac{RT}{\left(F_{z_Y}\right)\ln\left([Y]_o/[Y]_i\right)}$$

where R is the universal gas constant, T is the temperature in Kelvin, is F the Faraday constant, $z_Y$is the valence of ion Y, and $[Y]_o$ and $[Y]_i$ are the concentrations of ion Y outside and inside the membrane, respectively. (42)

There are also other ways to transport the ions across the membrane, using pumps and exchangers. The most important ones are the Na^+/K^+ pump and the Na^+/Ca^{2+} exchanger. The Na^+/K^+ pump extrudes Na^+ that enters the cell from the fast Na^+ channels by transporting three Na^+ ions outside the cell and two K^+ ions inside. Under normal

circumstances the Na^+/Ca^{2+} exchanger operates primarily to extrude Ca^{2+} ions from the cytoplasm by exchanging one Ca^{2+} ion for three Na^+ ions

This behaviour of the ionic currents is similar in neuronal and cardiac cells. Due to this fact, the first models were based on the Hodgkin-Huxley (43) model. There are various important models that simulate the myocytes cell using differential equations. They are based on animal experiments and they describe the behaviour of the membrane, ionic pumps and intracellular components. Some of the most famous and generic models are:

- Beeler-Reuter model: This model was created in 1977 and takes into account 4 of the 8 ionic currents known at that moment. It implemented a fast inward Na^+ current I_{Na}, the time-dependent outward current I_{x1}, a time-independent K^+ outward current I_{K1}, and a slow inward current Is carried primarily by Ca^{2+} (5) (44).
- Luo-Rudy model: The Luo-Rudy model 1 is based on the previous model but it includes the new observations made at that time (1991). Now, there are 6 ionic currents present in the model. In 1994, some modifications were included in the model, and some of the currents were described in more detail. Therefore, the number of currents involved in the model was now 11. The final model arrived at 1995, when dynamic components were added to the model to make it possible to change over time. (7) (6) (44)
- Fenton-Karma model: was developed in several papers in 1998 and 2002. It is known as the 3V-model because it uses three transmembrane currents: fast inward Na^+, slow inward Ca^{2+} and slow outward K^+. In addition there are several parameters that can be set to adjust the results to the experimental data. These parameters are the threshold for excitation, action potential rate of rise, minimum diastolic interval, minimum and maximum action potential durations, and action potential duration and conduction velocity restitution curves. (8)

Most of the time the models have been done based on animal studies (45) (46) (47) (48) but there are some human models for some types of cells adapting the model to the human data that was available at that time. For example, there are human atrial cell models as the one shown by Courtemanche et al. in 1998 (49) based on Luo-Rudy model or the one described by Simitev and Biktashev in 2006 (50) which is based on the previous one and reduces the number of variables. There are human models for ventricular cells also based on Luo-Rudy model as the one published by Priebe and Beuckelmann in 1998 (51) and its reduction published by Bernus et al. in 2002 (52). Other models show different approaches as the Iyer-Mazhari-Winslow model (53) which follows a Markov chain approach or Ten Tusscher et al. (2004) (54) which shows

a full description of the calcium dynamics. There are no human models for the SA node but there are many models for rats and rabbits.

2.2.2 Modelling of the electrical conduction in cardiac tissue

The heart and the heart tissue can be modelled as a system with distributed elements that interact among each others. The dynamic of each element of the tissue and the interactions among each other can be classified depending on the variables that take part into the model (macroscopic and microscopic) or the mathematical formulation used to describe them (differential equations and cellular automata).

When a microscopic model is used, the information available is at cellular level. The region is divided in different areas and each one is assigned as intracellular, extracellular or to the membrane. Each area has an electrophysiological description and the current flow among them is modelled with the Ohm law. If the only domain of interest is the intracellular space, monodomain models are used. Bidomain model are used to work with the intracellular and extracellular space. The main problem of these models is that they can only be applied in small areas due to the need of a large computational power. On the other side, the macroscopic approach combines the cells to be treated in a common way and the electrophysiological variables of the tissue are the ones taken into account.

The macroscopic models can be divided in different groups depending on the approach that is used. There is a more mathematical method called reaction diffusion equations and there is another computer science based technique known as cellular automata.

Reaction diffusion systems

The reaction diffusion systems are based on differential equation systems that describe the excitation and propagation through the medium. There are different kinds of models that can be grouped as:

- Simplified approaches
- Combinations of electrophysiological cell models with electrical current flow models
    - Monodomain
    - Bidomain (44)

SIMPLIFIED MODELS

The simplified models are based on generic excitable media models. The most famous simplified model is the one developed by FitzHugh and Nagumo in 1961 (9) and it can be described as:

$$\frac{\partial u}{\partial t} = \frac{u - \frac{u^3}{3} - v}{\epsilon} + D\nabla^2 u$$

$$\frac{\partial u}{\partial t} = \epsilon(u + \beta - \gamma v)$$

Where u is the transmembrane voltage and v is the state variable for inhibition. D is the diffusion coefficient and the typical parameters are $0 < |\beta| < \sqrt{3}$,$0 < \gamma < 1$ and $\epsilon \ll 1$. (9)

This model can represent the general propagation and excitation properties, but it is not able to represent many other properties as the rate dependence of the action potential among others (42). There are some modifications of this model as the one presented by Roger and McCulloch which allows more realistic descriptions of the propagation (10).

MONODOMAIN MODELS

The monodomain models show the propagation in the intracellular space. It can be represented as set of resistors and voltage sources (Figure 2.12). It uses the cell models as a voltage source which is connected to the neighbouring cells by resistors.

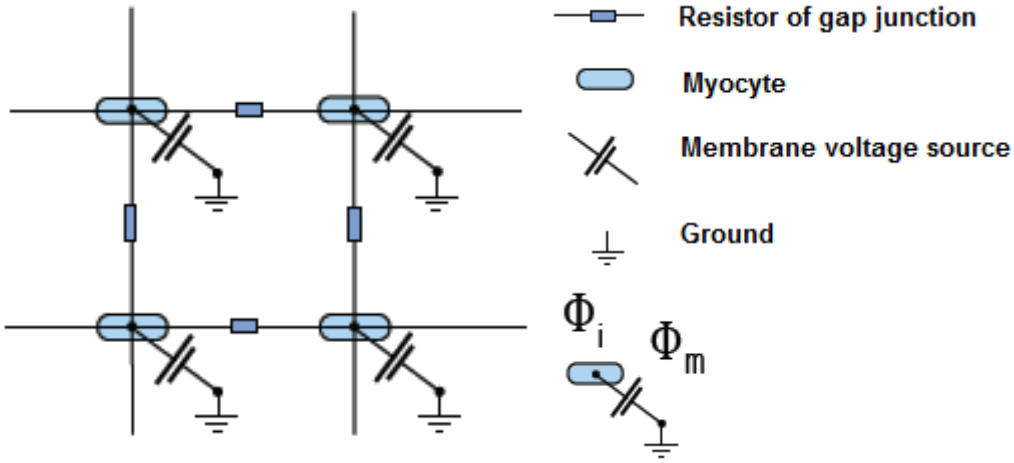

Figure 2.12. Graphical representation of monodomain model. (44)

When one of the cells is excited, it will increase the voltage in that point. The current will flow to the neighbouring cells through the resistor network. If it is sufficient to raise the voltage over the threshold to open the sodium channels, it will excite this cell and the propagation will flow from cell to cell. (44)

The mathematical description of this model is done using the Poisson equation. This equation shows the relationship between the gradient of the transmembrane voltage V_m and the source currents f_i.

$$\nabla \cdot (\sigma_i \nabla V_m) = f_i$$

Where σ_i is the intracellular conductivity.

The intracellular source current comes from the intracellular source current f_{si} and the transmembrane current I_{tm} where β is the myocytes per volume ratio.

$$f_i = \beta I_{tm} - f_{si}$$

The transmembrane I_{tm} current is described by the electrophysiological cell models which depend on the membrane voltage V_m and the ionic currents I_m where C_m is the transmembrane capacitor.

$$I_{tm} = C_m \frac{\partial V_m}{\partial t} + I_m$$

Combining these three equations, we obtain the general equation for a monodomain model:

$$\nabla \cdot (\sigma_i \nabla V_m) = \beta \left(C_m \frac{\partial V_m}{\partial t} + I_m \right) - f_{si}$$

This can be written in a different way which is easier to apply numerical methods as finite differences or finite elements methods.

$$\frac{\partial V_m}{\partial t} = \frac{1}{C_m} \left(\frac{f_{si} + \nabla \cdot (\sigma_i \nabla V_m)}{\beta} - I_m \right)$$

BIDOMAIN MODELS

The bidomain model is an extension of the monodomain model including the extracellular domain. It is useful for applications as defibrillation or pacemakers which need to know the propagation in the extracellular space. For pure conduction behaviour, the monodomain models are enough. (44)

Now the voltage source is coupling the intracellular and extracellular domain. There will be two pathways for the currents, the intracellular grid and the extracellular one which have different resistor values. The idea of this model is to separate the

calculations of both domains that will be coupled just by the voltage sources, as it is shown in Figure 2.13.

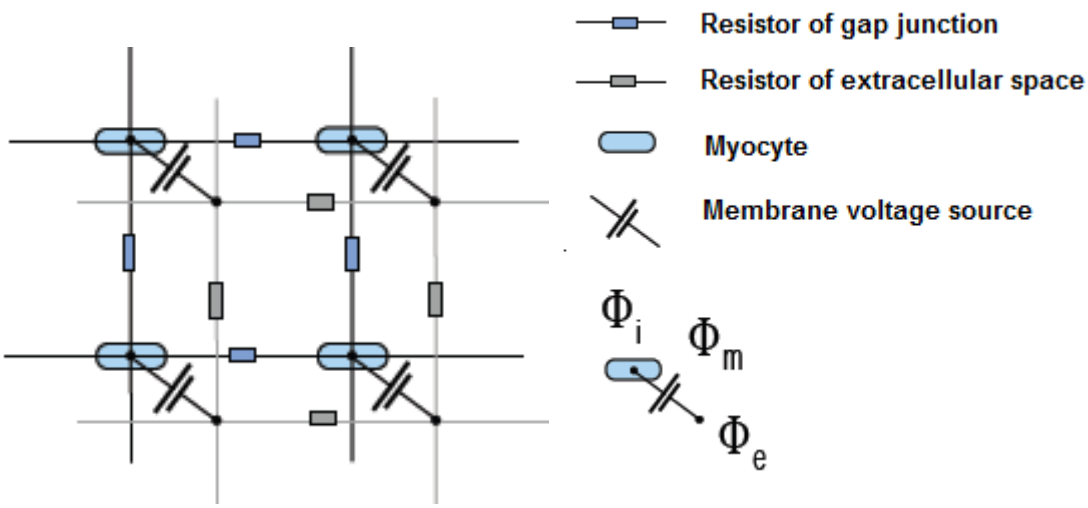

Figure 2.13. Graphical representation of bidomain model. (44)

Both domains are separated having their one Poisson equations.

$$\nabla \cdot (\sigma_i \nabla \phi_i) = \beta I_{tm} - f_{si}$$
$$\nabla \cdot (\sigma_e \nabla \phi_e) = -\beta I_{tm} - f_{se}$$

with the intracellular potential ϕ_i, the extracellular potential ϕ_e, the intracellular conductivity tensor σ_i, the extracellular conductivity tensor σ_e, the intracellular stimulus current source density f_{si}, the extracellular stimulus current source density f_{se}, and the myocyte per volume ratio β.

These two equations are coupled by the transmembrane voltage:

$$V_m = \phi_i - \phi_e$$

Adding both equations we obtain:

$$\nabla \cdot (\sigma_i \nabla \phi_i) + \nabla \cdot (\sigma_e \nabla \phi_e) = -f_{si} - f_{se}$$

which can be solved using numerical methods.

The anisotropy can be added to these models changing the values of the resistors. But the problem is that they required a big computational load to be able to solve the differential equation system. This computational load can be minimized with the cellular automata. (44) (55)

Cellular automata

Cellular automata are based on state machines with some specific rules for the transition from one state to the other. The medium is divided as a cell array where each cell has a finite number of states and they change from one state to another depending on the interaction with the neighbour cells.

Figure 2.14 shows a simple automaton. There is a geometry with active elements and an initial excitation is created. The rules are defined allowing the propagation to all the neighbours to the excited cell. After one cycle the cell of the initial excitation changes its state to just excited (in yellow colour) and after four cycles is comes to the rest state again. This figure shows a simple propagation with a very simple set of rules.

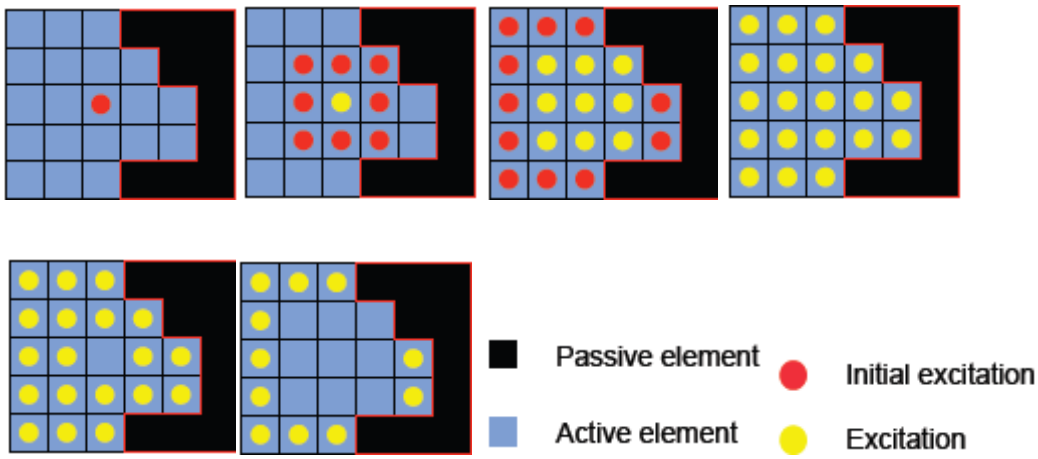

Figure 2.14. Example of a simple cellular automaton.

The elements needed to build a cellular automaton are:

- Spatial domain: a really detail description of the geometry to be used.
- Physiological information: this information can be action potential, conduction velocity or refractory period among others. There are other kinds of properties that are neglected as the ion concentration or the extracellular potentials.
- Set of rules: These rules represent the way the automaton is going to behave. They represent the conduction mechanism in a simple manner. (44)

There are different kinds of automata depending on the number of neighbours. The neighbour number is the one setting the shape of the wave front. For 3D simulations, there are 6- and 26- neighbourhoods, while for 2D, there are 4- and 8- neighbourhood. (44). Figure 2.15 shows the two possible sets of neighbourhoods for a 2D simulation.

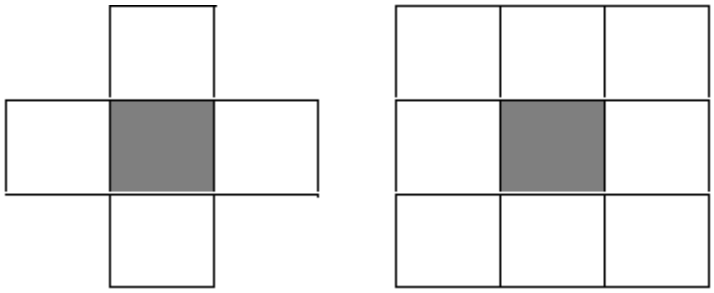

Figure 2.15. Representation of 2D neighbourhoods; a) 4 neighbours and b) 8 neighbours.

The first automata were done as graphical methods on paper using simple geometries. Wiener and Rosenblueth were able to describe the propagation around an obstacle just describing a simple set of rules which were applied graphically (56). The first computer simulation was carried out by Moe et al. in 1964 showing atrial fibrillation (11).These early versions were simple and they could not describe complex phenomena. Nowadays, the automata models have increase their expressive capacity and they do not require as much computational load as the differential equation models (57) (58). There are models as the ones developed by Wei et al. in 1995 and Werner et al. in 1998 that shows 3D simulations of the whole heart taking into account the anisotropy of the tissues (59) (12).

In its model, Wei included 16 different types of cell to include infarction, ischemia, ectopic beat and others. It uses a curve to correct the value of the action potential in different situations and another timing curve to control the refractory period of the cells. The main limitation of this model was the resolution which did not allow the studies of small re-entries. (59)

Werner's model is a 3D automaton which can work from small areas of the myocardium to the whole heart. The number of neighbours is fixed to 26 in most of the cells, but the ones corresponding to the conduction system tree where the number of neighbours varies from one to another. This model was able to simulate spirals and blocks and atrial and ventricular flutter in the whole heart. (12)

2.2.3 Electrical signals modelling

The action potentials generated in the cardiac cells can be recorded as electrograms (EGM). This electrograms can be modelled in different ways. For this work, the models that will be used are the one based on lead fields.

To be able to define the lead field theory, first the concept of lead vector and the reciprocity theorem should be introduced. But before this, the forward problem should be described.

The forward problem describes the relationship of the field recorded in a volume conductor (e.g. thorax) with the source (e.g. heart). The human body has a conducting properties and it is able to conduct the electrical signals which are generated in the heart or the brain. The tissues have resistive and capacitive behaviour but at low frequencies it is mainly resistive. Therefore, a quasistatic approach can be used which means that the currents and fields behave as stationary at any instant of time. This allows using the Poisson and Laplace equations to describe the relationship of the fields with the sources. In this case, the source is the cell which creates the beating and the volume conductor is the other cells which propagate the signal. (4)

The lead vector concept explains the relationship between electromotive source and the measured voltage. We want to calculate the potential field at point *P*, generated by a unit dipole *i* at a location *Q* aimed to x-axis direction. The potential field generated by this unit dipole would be c_x.Taking into account the linearity principle, the potential field generated by other dipole p_x would be $c_x p_x$ (Figure 2.16).

The same idea holds for the other two directions *y* and *z*. And applying the linearity principle once again, for any arbitrary dipole the potential field at *P* would be:

$$\Phi_P = c_x p_x + c_y p_y + c_z p_z = \bar{c}.\bar{p} \quad (2)$$

This vector $\bar{c}$ is called the lead vector for a unipolar lead.

When the potential is measured between two points (the reference is not remote), we are talking about the bipolar lead. In this case the potential fields for point P_i and P_j are:

$$\left.\begin{matrix} \Phi_{P_i} = \bar{c}_i.\bar{p} \\ \Phi_{P_j} = \bar{c}_j.\bar{p} \end{matrix}\right\} \Rightarrow V_{ij} = \Phi_{P_i} - \Phi_{P_j} = \bar{c}_i.\bar{p} - \bar{c}_j.\bar{p} = \bar{c}_{ij}.\bar{p} = \bar{c}.\bar{p} \quad (3)$$

Therefore, in the bipolar lead context, *c* is the lead vector calculated as the difference of lead vectors at each point.

Thus, the lead vector depends on:

- The location *Q* of the dipole $\bar{p}$

- The location of the field point *P*
- The shape of the volume conductor
- The (distribution of the) resistivity of the volume conductor

The concept of lead field is an extension of the lead vector. The lead field can be explained as a continuous vector field made up single leads vector as a function of the source location through the volume conductor. The reciprocity theorem serves as the basis for the lead field theory, which provides a powerful way to evaluating and interpreting measured signals in terms of their sources.

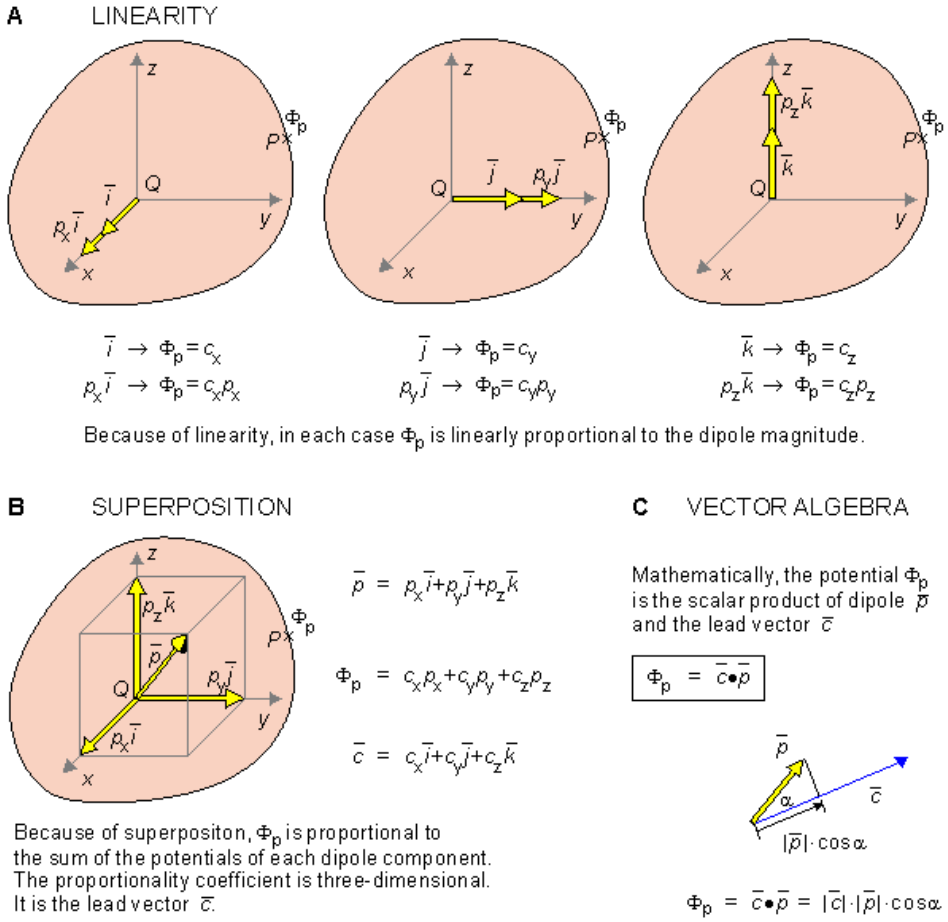

Figure 2.16 Lead vector concept. Any vector can be described as a superposition of three components in the direction x, y and z. a) Describes the magnitude of each lead vector for each component. b) Applying the superposition principle, the lead vector p is shown as a linear combination of its components. c) This linear combination can be expressed as a dot product operation. (4)

Normally, voltage measurement is made on the surface of the volume conductor and the measured signal in the lead arises from all the sources in the conductor according to the previous equation at each location. The reciprocity theorem states that electrical field E inside the volume conductor generated by a reciprocal unit current I_r applied to the surface electrodes expresses how the same electrodes record potentials caused by dipole sources at any location within the volume conductor. Thus, the associated current density field $\bar{J}^i$, noting that $J = \sigma E$, the expression for lead potential becomes

$$V_{LE} = \int_v \bar{c} \cdot \bar{p}\, dv = \int_v \frac{1}{\sigma} \bar{J}_{LE} \cdot \bar{J}^i\, dv \quad (4)$$

Where $\bar{J}_{LE}$ denotes the lead field and σ is the electrical conductivity tensor unique for each location and direction. (4)

2.2.4 Numerical methods

There are several numerical methods to solve the Poisson equations. These methods are the finite element method (FEM), the finite difference method (FDM) and the boundary element method (BEM).

FINITE ELEMENT METHOD

Finite element method is a standard method to solve physical problems. It allows taking anisotropy, inhomogeneity and nonlinearity of material properties into account. The spatial domain is discretised in finite elements. The interpolation functions are selected to find how the field variables are distributed in the elements starting from a specific node. With the mathematical description of the field problem, the element matrices that describe energy in each element for given node variables is set. These element matrices are combined in a system matrix. This matrix and the boundary conditions will define a linear equation system. Its solution is the description of the field function over the whole domain. It assigns the value at each element and using the interpolation function the result over the continuous domain can be found. (44)

The major complication of this method is the definition of the mesh for the geometry. It takes the major computational load. But it gives more accurate results in the boundaries, because the mesh can be deformed to fit the geometry as much as it is needed. (60)

FINITE DIFFERENCE METHOD

In the FDM, the domain is discretised in points which are the corner of cubical elements forming a resistor network. The network is described as a set of partial differential

equations showing the currents and potentials in each node of the model. This description defines a node vector for each point. All these vectors are assembled into a system matrix which will define a linear equation system with the help of the boundary conditions. The solution of this system is the field function which gives the value for each point. (60) (44)

In this case the solution is defined at the nodes while in FEM the solution has to be interpolated to the elements between the nodes. The main drawback is the problems defining the tissues boundaries. As the mesh is a fixed grid, there are problems approximating complex boundaries with the pixels. (60) (55)

BOUNDARY ELEMENT METHOD

This method considers the interior of the boundary as homogeneous and the interest region is just the boundary. The boundary is the only region divided into elements. The BEM approximates quite accurately complex surface shapes and it is suitable for surface approximations. (61)

3 Materials and Methods

The main goal of this thesis is to create a model of the electrical activity of the cardiomyocytes to analyze the different behaviour for the different types of cells. To perform this task, we have created a cellular automaton that needs the geometry of the cells and its lead field for the specific geometry and for the specific measurement configuration as an input.

In this chapter, there is a description of the setup used in the laboratory to record the real signals from the cardiomyocyte. The different parts of this system which need to be modelled in the computer to obtain a similar signal to the recorded one in the laboratory are also explained. Finally, the basic simulations to proof the functionality of the cellular automata and its setups are also presented.

3.1 Laboratory setup

The system used in the laboratory to record the signals from the cell culture is a microelectrode array (MEA) system manufactured by Multi Channel Systems (MCS GmbH). This MEA system includes a MEA, an amplifier and a software to record the measured data (Figure 3.1).

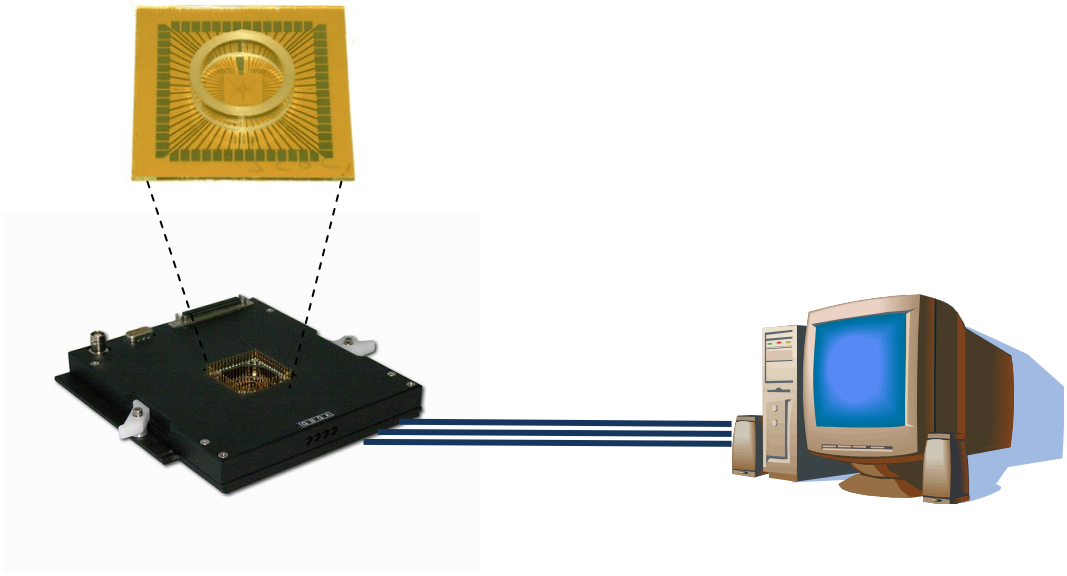

Figure 3.1. Diagram of the laboratory setup with the MEA, the amplifier and a conection to a computer to record the data in the specialized software.

The MEA used in the Regea laboratory is the model MEA200/30iR-Ti-gr. It has a grid of 8x8 electrodes with a diameter of 30 µm and a distance between the electrodes of 200 µm (Figure 3.2). The electrodes are made of Titanium nitride with tracks of Titanium. They are situated over a base of glass with silicon nitride as an insulator. (62)

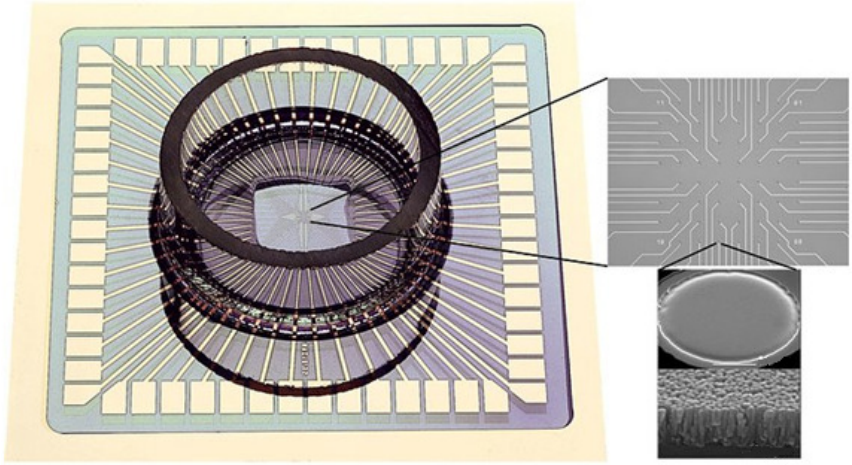

Figure 3.2. Image of a multielectrode array from Multichannel systems with a detail of the electrode.

The amplifier used in the laboratory is the model MEA1060-Inv-BC from Multi Channel Systems (63). The main characteristics of this amplifier which will be used in this thesis is: a) a gain of 1100 ; b) a bandwidth from 10Hz to 3KHz. It is designed for inverted microscope and it has a blanking circuit to avoid the saturation of the amplifier. The signals are sent from the amplifier to the computer which uses the software MC_Rack to record the electrical signals.

3.2 Modelling of the laboratory setup

The different parts of the laboratory setup have to be modelled in the computer to obtain the simulated EGM. First, the geometry of the cell culture and the lead fields for the electrodes have to be modelled. These will be the input for a cellular automaton which describes the electrical propagation in the tissue. With currents calculated in the automaton and the help of the lead fields, the EGM are calculated obtaining a simulation of the output of the electrodes from the MEA. After the MEA the signal is amplified to be recorded in the computer. The transfer function of the amplifier will be modeled in Matlab to filter the EGM and obtain this simulation.

3.2.1 Generation of the geometry for the model

To generate the geometry model of the cells and to obtain the lead fields, there are several steps to follow:

1. Acquisition of the anatomical data of the cells.
2. Segmentation and discretization of the image to obtain the different types of objects and tissues.
3. Create the FDM model of the segmented data.
4. Solve the FDM model to find the lead fields at each point for the position of the electrodes.

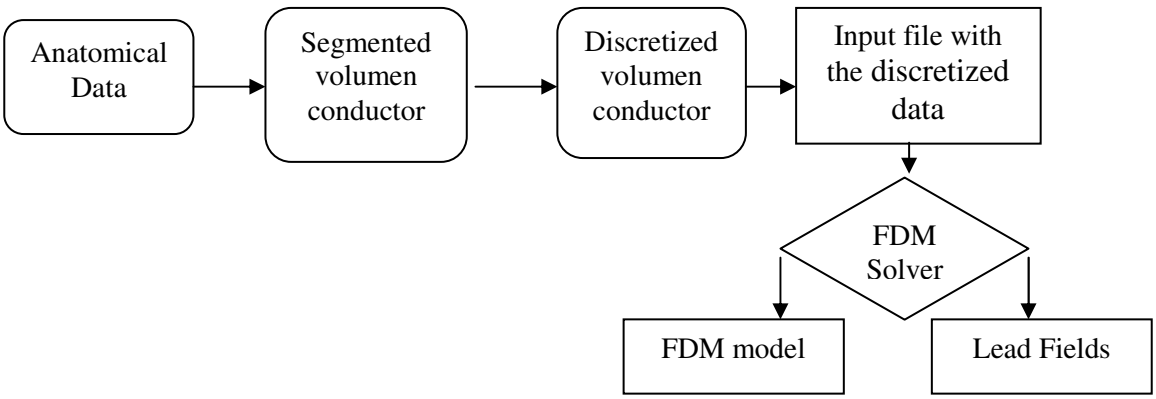

Figure 3.3. Flow diagram with all the steps to obtain a FDM model from the anatomical data.

The acquisition of the anatomical data was performed in the Regea Institute of Regenerative Medicine where microscopic pictures of the cells were taken. This data was segmented using a simple free software program (GIMP) for manipulation of images. This segmented data and the dimensions of the measurement instrument were introduced in Matlab to process it and create a 3D model of the experiment that was performed in the lab.

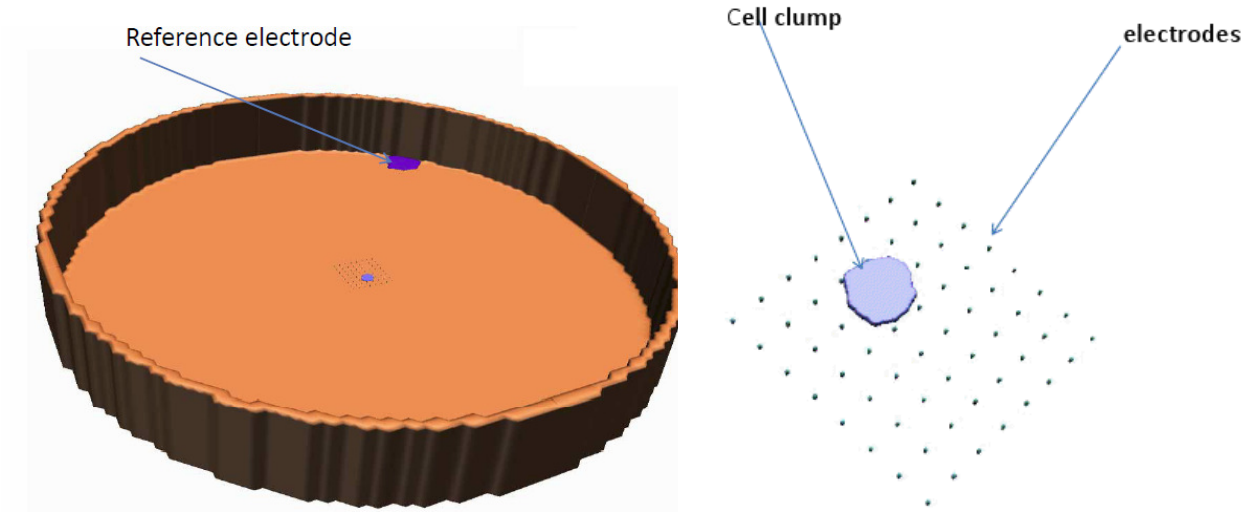

Figure 3.4. Illustration of the 3D model created in Matlab from the cell culture images obtained in the laboratory.

The model in Figure 3.4 shows the Petri disc were the cells are placed, the MEA electrodes which record the signals from the cells, the medium were they grow and the cells itself.

The FDM input files are generated with the model created in Matlab. The solver used for the finite different method was implemented by Takano (64). The solver gives electric fields within the elements of the model.

The model used has 64 layers separated by 0.01mm. To have a good solution for the lead fields without obtaining too many elements, there were two different resolutions in the model. The resolution in the region of interest is 0.01mm and 0.05mm in any other part. The region of interest is a 4mm x 4mm square centered over the electrodes. Each electrode will be modeled as a square of 0.02mm x 0.02mm.

There are several inhomogeneities in the model. There is the glass from the Petri disc, the medium, the electrodes which are made of Titanium Nitride and the cell culture. The resistivity values which were applied in the model for each of them are shown in Table 3.1.

Table 3.1. *Resisitvity values for each of the inhomogeneities of the model*

Inhomogeneities	*Resistivity (Ω·cm)*
Medium	*654*
Glass	*100000*
Cell culture	*50*
Electrodes (Titanium Nitride)	*0.0013*

3.2.2 Description of the cellular automata model

The cardiac model used for the propagation of the electrical activity in this thesis is a cellular automaton based on the restitution curves including a probabilistic component. The changes in the automaton from one state to another are not made in a deterministic way. This model has not been developed in this thesis. It was already developed by Felipe Alonso *et al.* in 2005 (13). It has been used as the core algorithm for the propagation of the electrical activity in the tissue, but there have been some modifications to suit the needs of this software.

The cardiac tissue is modelled as an array of cells where each cell can hold three different states: *rest, refractory1* and *refractory2*. Figure 3.5 represent the transitions from one state to another. When the cell is at *rest*, it can be excited by the neighbour cells. The cell will continue in the same state until it receives a stimulus big enough. Once it has been excited, there is a depolarization in the cell and its new state is *refractary1*. The cell will be in this state during the *F* fraction of the action potential duration (APD). Now that the cell is excited, it can excite the surrounding cells. After the *F* fraction of APD, the cell will be in the state *refractary2* in which the cell is excited but cannot excite any other cell. When the whole time of APD is concluded, the cell comes to the *rest* state.

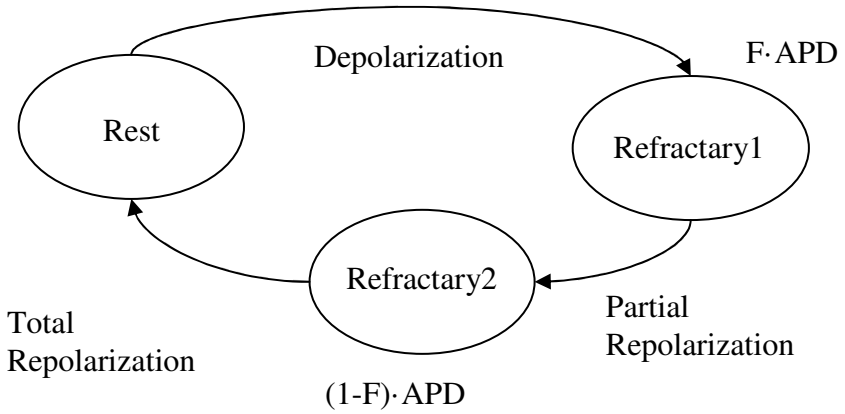

Figure 3.5. Cellular automata diagram of states.

As it can be observed, the transitions among the status *refractary1* and *refractary2*, as well as, among *refractary2* and *rest* state, are done in a deterministic way according to the beating instant and the APD curve. The probabilistic component is included in the transition between the *rest* and the *refractory1* states. The transition will happen when the probability of excitation of cell *j* is bigger than a threshold. The probability of excitation is described as:

$$P_j^{exc} = E \cdot Q \quad (7)$$

where the excitability of the cell (E) depends on the conduction velocity (CV) of that cell and the amount of excitation around the cell (Q) depends on the restitution properties of the APD in the neighbour cells. (13)

The excitability is calculated taking into account the CV and the conductivity of neighbouring cells, as well as the conduction velocity. To have the probabilistic component the threshold is calculated as a random number.

There would be a change in the state of the cell when the result of the multiplication would be greater than the random number.

The value of the APD, as well as the value of the CV, depends on the diastolic interval (DI), the time between to excitations in the cell. The APD and the CV get bigger when the interval between depolarization increases. The curves of the APD and CV versus DI are introduced in the program as input parameters.

The excitation will be only generated in the cardiac tissue, because the cells are the only ones that are able to generate electrical activity by themselves. The point where the excitation will start is marked by the beating coordinates or the ectopic coordinates in the main view of the program. The output of the automaton is the voltage at each element of the model in each instant of time.

3.2.3 Calculation of EGM with Lead Fields

As it was explained in chapter 2, the voltage at an electrode can be calculated with the lead field theory as:

$$V_{LE} = \int_v \bar{c} \cdot \bar{p}\, dv = \int_v \frac{1}{\sigma} \bar{J}_{LE} \cdot \bar{j}^i\, dv \quad (4)$$

where $\bar{J}_{LE}$ denotes the lead field, $\bar{j}^i$ is the impress current and σ is the electrical conductivity tensor unique for each location and direction.

To calculate the impressed current that is differential of current between the cells, the ohm's law is used. The differential voltage at each point is calculated as a difference with the neighbour nodes, and then is multiplied by the connectivity to obtain the current. Therefore, the EGM is calculated as a sum of all components of the multiplication of the current and the lead fields.

As the impressed current is depending on the source and it can be calculated at the beginning. Then the different voltages can be calculated for the different electrode with less computational charge, because the current will only be calculated once, and that is the most time consuming.

3.2.4 Modelling of the amplifier

The EGM obtained from the previous steps is the one recorded at the electrodes of the MEA. In real life, measurement systems introduce some noise in the signals. Therefore, an amplifier is added to the system to reduce some noise and amplify the signal before it is acquired by the computer. To model this effect in our simulations, some random noise is added to the signal resulting from the previous step to resemble the noise introduced by the electrodes. The amplitude of the random noise is 20% of the maximum amplitude of the signal. The amplifier is modelled in Matlab using the characteristic of the amplifier described in section 3.1. To implement it in Matlab, two Chebyshev filters are used combined its poles and zeros.

The first Chebyshev filter is a high pass filter with a cut off frequency of 10Hz and order 1 to obtain a -20db/decade fall (Figure 3.6).

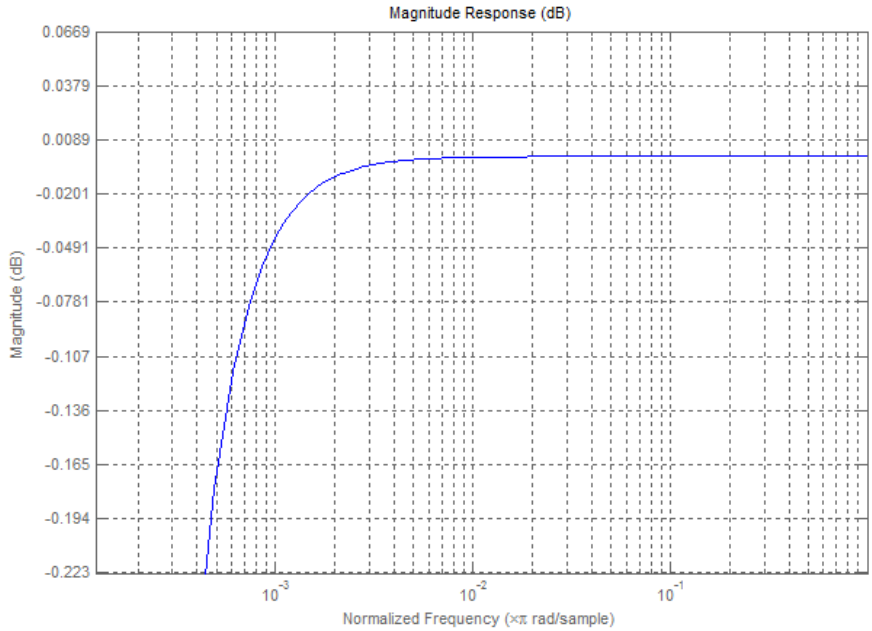

Figure 3.6. Magnitude representation of the Bode Diagram for a first order high pass Chebyshev filter with a cut off frequency of 10Hz. The frequencies are normalized to the sampling frequency, 20KHz.

The second Chebychev filter is a low pass filter with cut off frequency of 3KHz and order 3 because a slope of -60dB/ decade is needed (Figure 3.7).

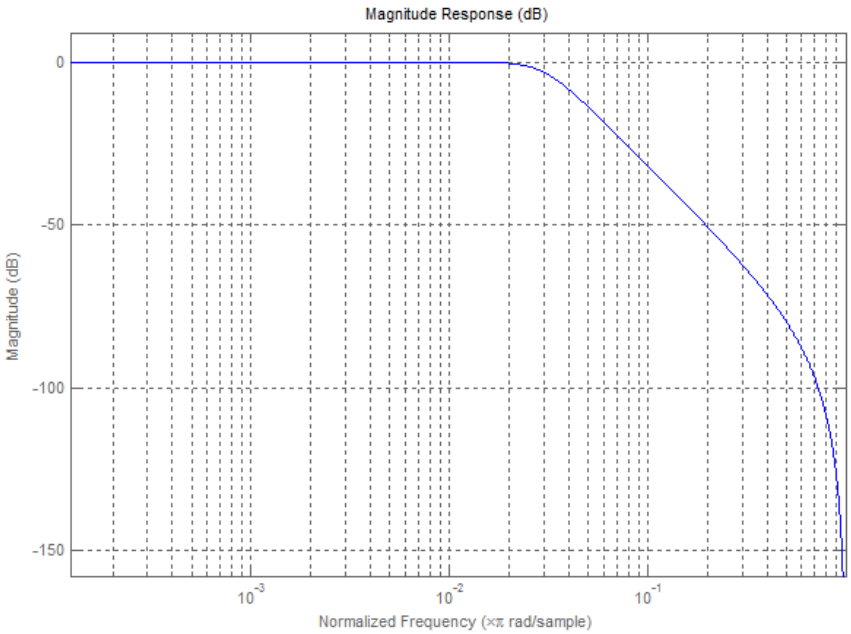

Figure 3.7. Magnitude representation of the Bode Diagram for a third order low pass Chebyshev filter with a cut off frequency of 3KHz. The frequencies are normalized to the sampling frequency, 20KHz.

Combining the poles and zeros of both filters, the specifications of the amplifier are found. When applying this filter to the signal a gain of 1100 will be add to obtain the gain specified for the amplifier (Figure 3.8).

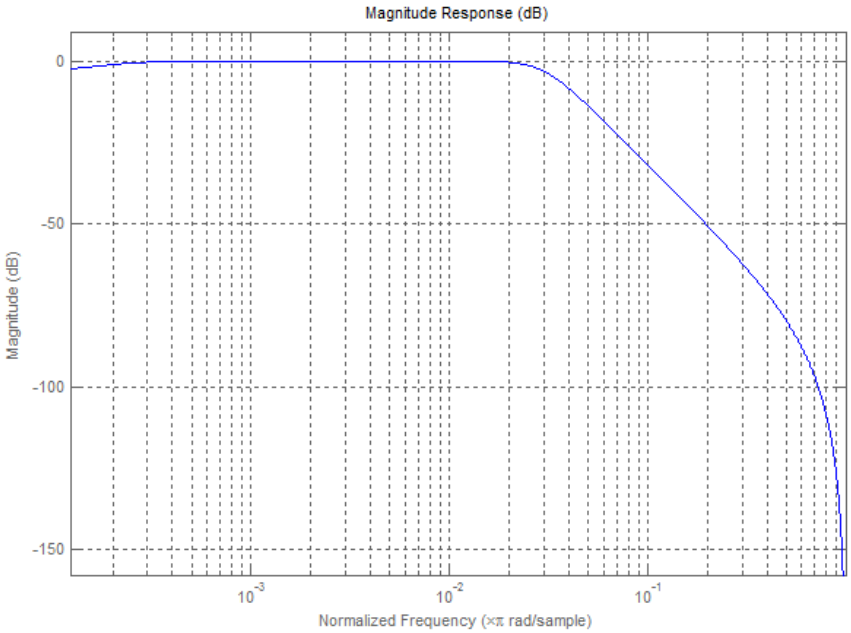

Figure 3.8. Magnitude representation of the Bode Diagram of the combination of previous two filters.

3.3 Simulations

Before doing any simulation, a study of the lead field would be done to see if the same set of lead field can be used in every simulation or if we have to calculate them for each experiment. Then, there is a set of simulations to validate the cellular automaton. Once the automaton is validated, there are several simulations with different action potential.

3.3.1 Study of the lead fields

The lead fields are calculated for each specific set of electrodes and geometry of the cell culture. Therefore, if the electrodes are changed or the cell culture is different, the set of lead fields have to be calculated again. As the cell culture is small in comparison to the MEA, a study of the lead field will be done to see if the same set of lead fields can be used with a specific MEA independently from the cell culture.

The study is performed comparing the lead fields of the MEA with and without cell culture. In addition to this comparison, the half sensitivity area will be calculated. The half sensitivity volume is defined as the volume where the lead field has reached half of it maximum value (4). This would define the volume where most of the information comes from. In our case, we are looking at the layer from the model where the cell culture is. Therefore, we are in a 2D case and the area will be calculated instead of the volume.

3.3.2 Validation of the cellular automaton

The first simulations are designed to validate the automaton. The validation is made using a model of cardiac tissue with well known shapes, a strip and a cross, to observe the propagation of the wave front. The model used in these cases is shown in the Figure 3.9.

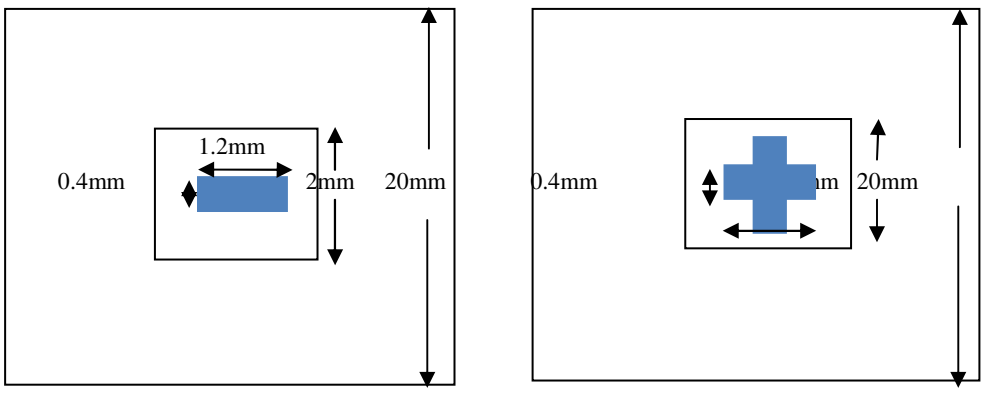

Figure 3.9. Simulation setups with the line and cross shape.

Two types of sources are used, point source and line source, in the left edge of the strip and the cross. The wave front should be arrow shape when the source is a point source and it should be a linear wave front when the line source is used. The electrode selected to observe the EGM is the electrode 29 in both cases because it is underneath the cross and the strip as it can be seen in Figure 3.10.

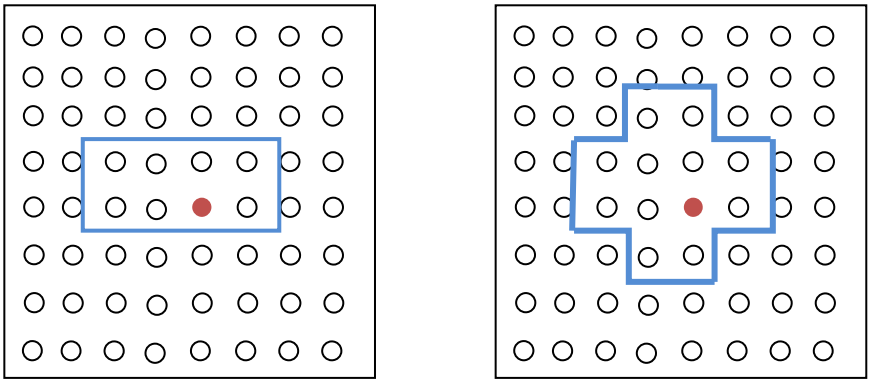

Figure 3.10. Position of the strip and cross setups with respect to the electrodes. The red electrode is the one used in the following section to show the results of the simulations.

3.3.3 Simulations with different action potentials

The second set of simulations compound the main objective of this thesis. I will try to observe some change in the EGM when all the conditions are maintained and the APD curves are changed. The APD curves for different types of cardiomyocytes are found in the literature (Figure 3.11). These curves are interpolated to be used as an input in the cellular automaton, introducing this curves as an input parameter of the program (Figure 3.12).

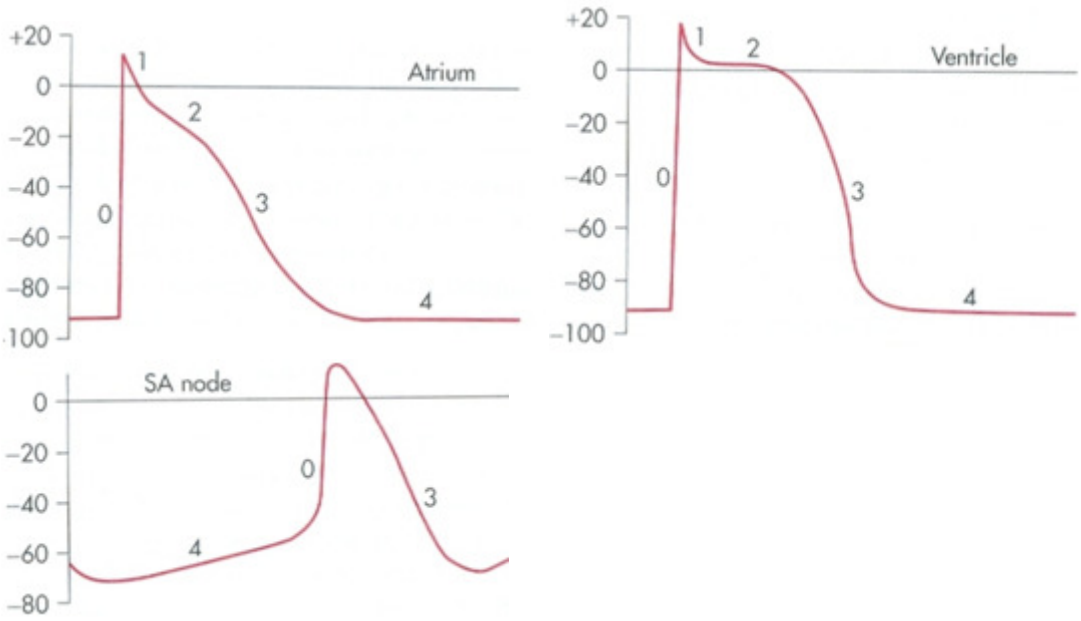

Figure 3.11 Action potentials for atrium, ventricle and SA node (16)

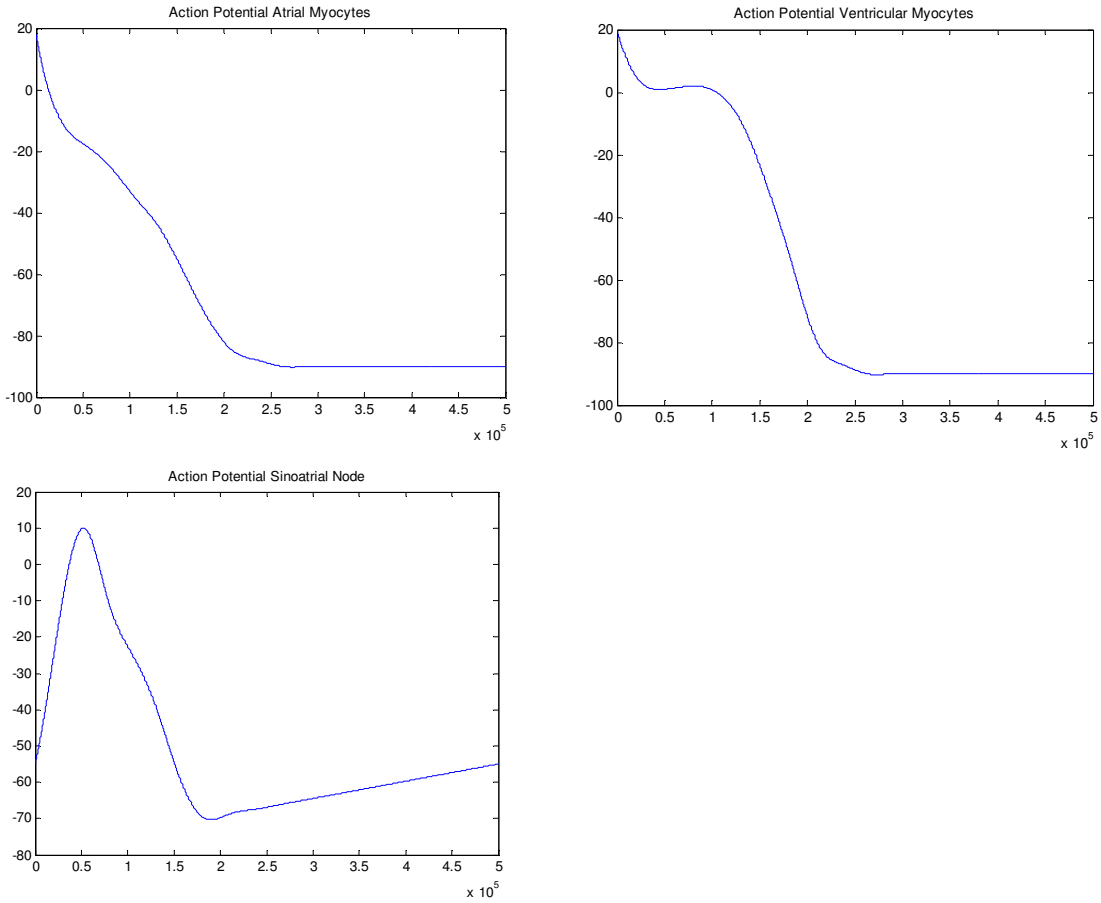

Figure 3.12. Action potential for the three different types of cells: atrial, ventricular, sinoatrial node used in the simulation.

These simulations will be performed in the same strip model as before and over the cell model (Figure 3.9 and Figure 3.4). In the case of the strip model, the electrode chosen to simulate the EGM is the electrode 29 as before, which is underneath the strip (Figure 3.10). When the cell model is used, the electrode chosen to observe the EGM is the electrode 53 (Figure 3.13.).

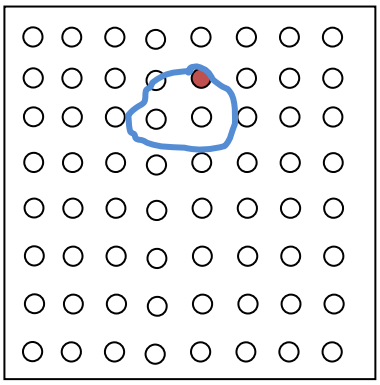

Figure 3.13. Position of the cell geometry with respect to the electrodes. The red electrode represents the electrode used in the result section.

To have a more realistic simulation, the last simulation will be done including the effect of the amplifier over a noise simulated EGM. A random noise will be added to the previous EGM obtained from the cell culture model and it will be used as an input to the amplifier to simulate the signal at the output.

4 Results

In this chapter the results from the different simulations will be shown. First, there is a small study about the lead fields obtained from the FDM solver. Then, there are some simulations to validate the model and finally a set of simulations for different APD curves.

4.1 Study of the lead fields

The purpose of the study of the lead fields of the electrodes provided by the FDM solver is to find the area of sensitivity of the electrodes and to see if the same solution for the lead fields can be use in all the cases.

As it has been said, the parameter to be calculated is the half sensitivity area. The radius of the area for each electrode is shown in appendix 1. Their values are 0.03mm for most of the electrodes which is the similar to the size of the electrodes (0.02mm x 0.02mm). Therefore each electrode is just aware of the electrical activity in their very close region. We can see this area graphically in Figure 4.1 and 4.2. Figure 4.2 shows the maximum value of any lead field for each point.

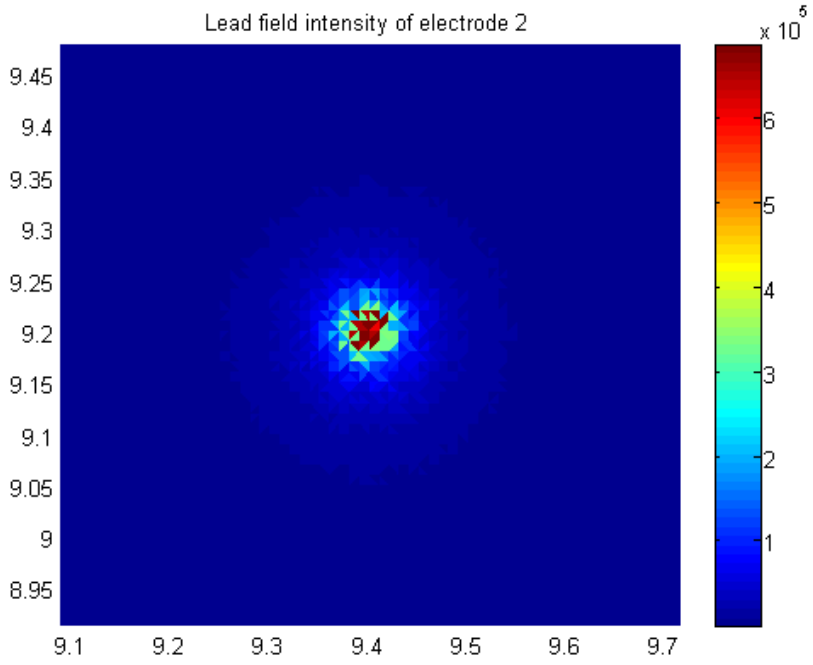

Figure 4.1. Lead field intensity electrode 2.

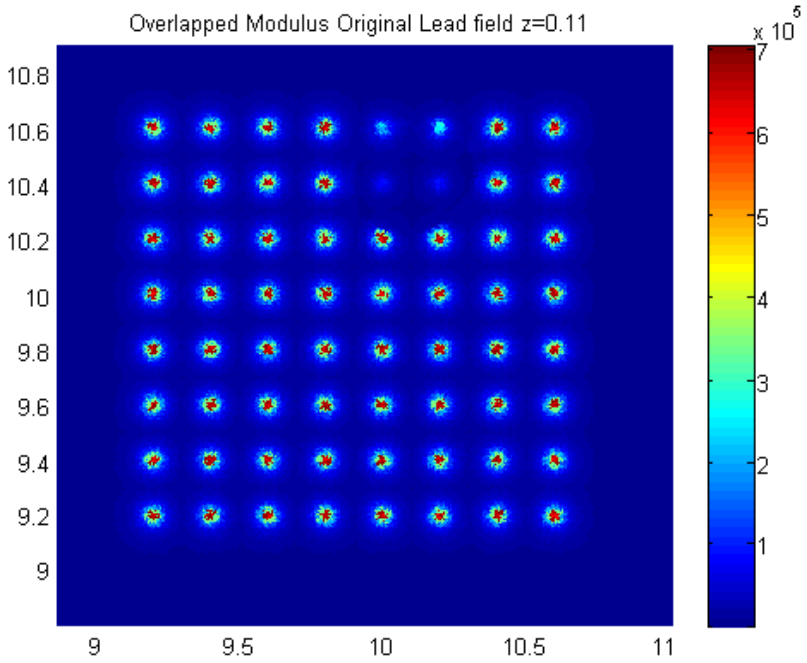

Figure 4.2. Lead field intensity whole MEA.

If there is an ectopic beat or a change in the propagation in areas that are not very close to the electrode, this electrode will not notice any change. In this Figure 4.2 we can notice that there are areas that are not well cover by the electrodes sensitivities. If there are some cells not conducting in the points between electrodes, it will not be noticeable from the EGM recordings.

One interesting feature to study was the effect of the conductivity of the cell culture in the lead fields. In Figure 4.3, the lead field for the original simulation with the cell culture is shown. Figure 4.4 shows the same model but eliminating the cell culture. Figure 4.5 shows the differences between both cases.

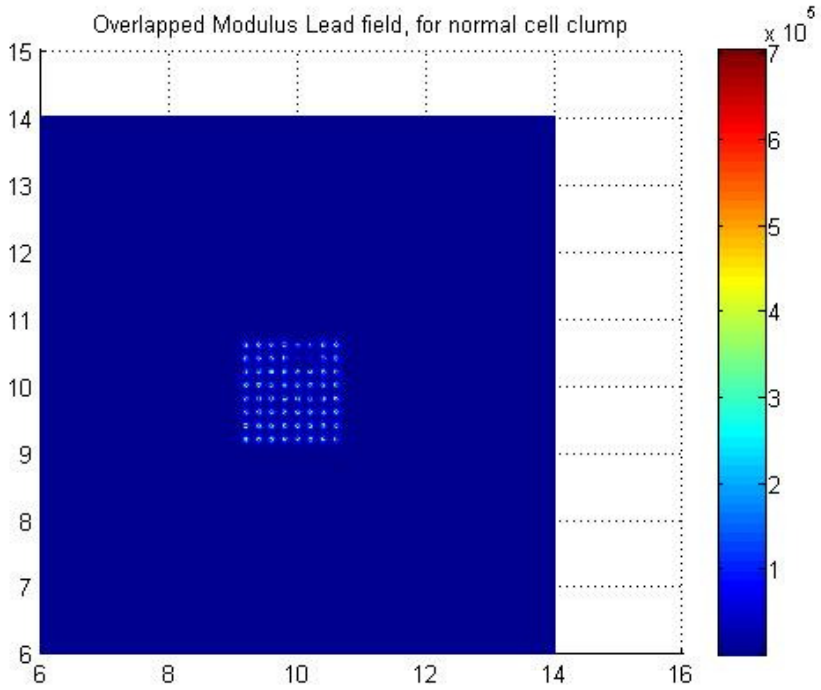

Figure 4.3. Lead field intensity when there is a cell culture over the electrodes.

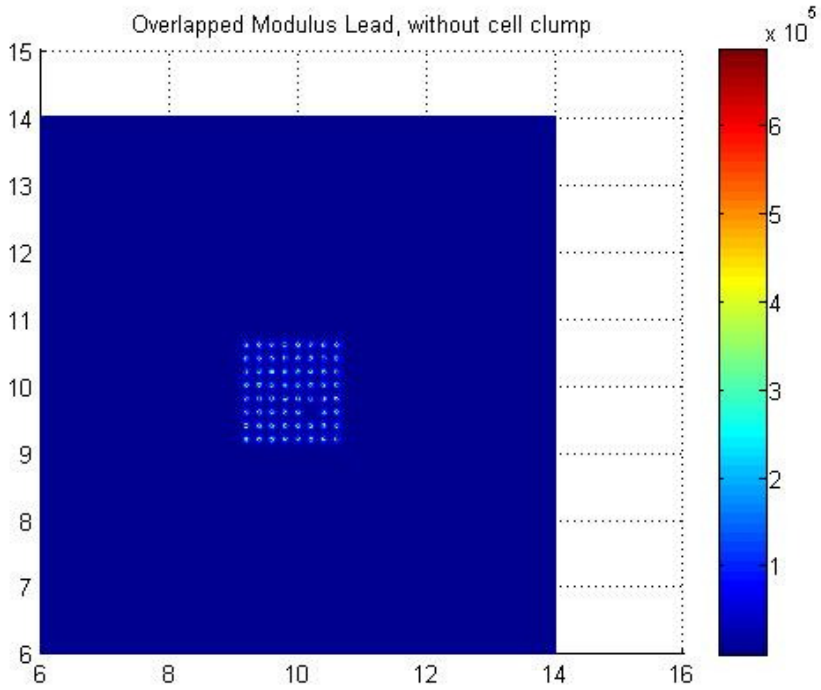

Figure 4.4. Lead field intensity when there is no cell culture.

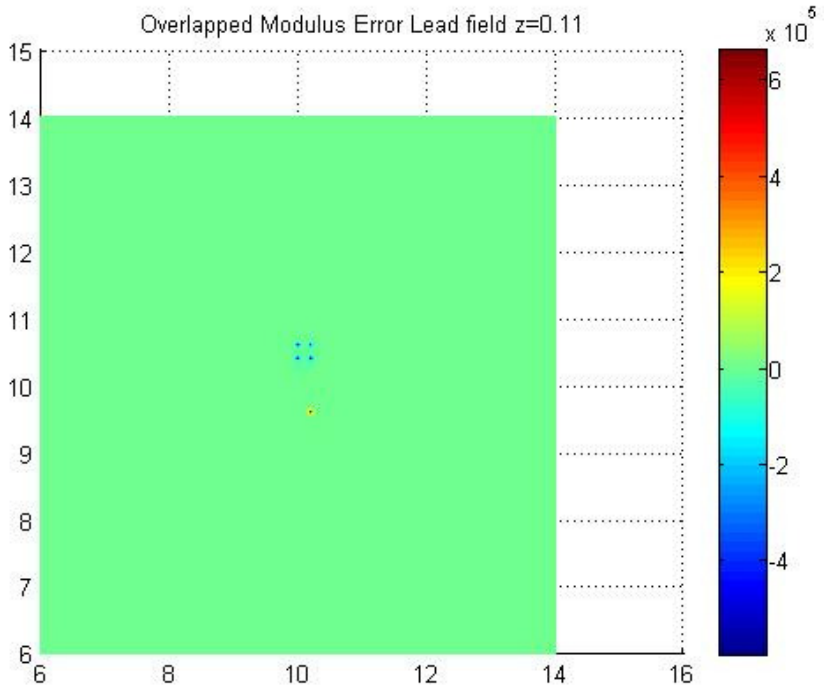

Figure 4.5. Difference in the lead field intensity between the cases with and without cell culture.

This difference can be shown as the percentage of change with respect to the lead field intensity without cell culture. It can be notice with a simple eye inspection that the lead fields from the electrodes where the cell culture is placed have lower intensity value. Table 4.1 shows this percentage for the electrodes where the lead field intensity differs.

Table 4.1. *Percentage of change in the amplitude of the lead field from the model with cell culture with respect to the model without the cell culture for the electrodes where there was a difference.*

Electrode	*Position (mm)*	*Percentage of change /%)*
60	*(10, 10.6)*	*-68.52 %*
61	*(10.2, 10.6)*	*-61.58 %*
52	*(10, 10.4)*	*-88.60 %*
53	*(10.2, 10.4)*	*-88.62 %*
22	*(10.2, 9.6)*	*2774.8 %*

The percentage of difference from the intensity of the lead field with cells in the culture to the intensity of the lead field without cells in the culture is around 70% and 80% less than the intensity of the lead field without cell (Table 4.1). Even though the cell culture is small with respect to the array of cells, the resistivity values for the media and the

cells are so different that there is a need to recalculate the lead field for each model with different geometry. It is not possible to use the same lead fields for a specific MEA when there are different cell cultures over it.

4.2 Validation of the cellular automata

The validation of the cellular automata is done according to the propagation. Two well known models (strip and cross) are used to see how the wave front behaves. To show the EGM, the electrode picked was the electrode 29 which is underneath the strip and the cross.

Figure 4.6 shows the propagation over a strip when there is a point source. This source was place in the midpoint of the left border of the strip (coordinate (9.5, 9.9)).

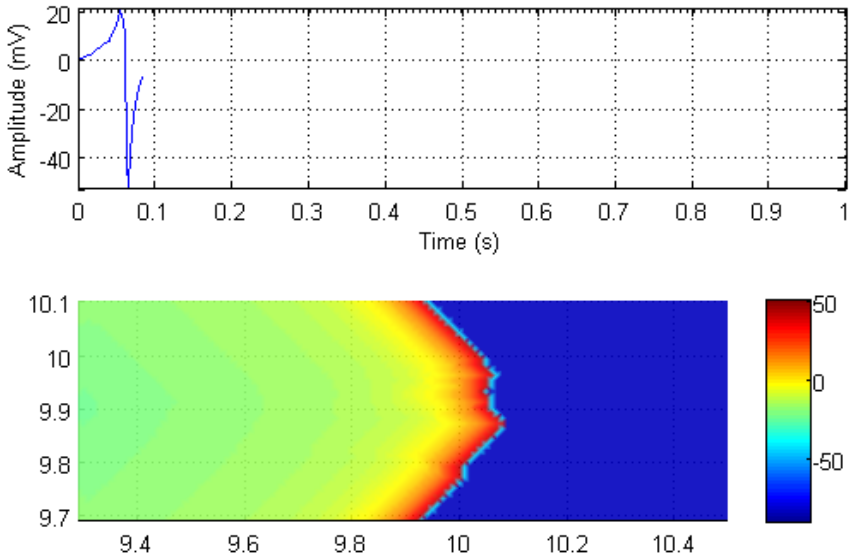

Figure 4.6. Propagation on a strip with a point source. The upper part shows the EGM recorded by the electrode and the lower part shows the propagation of the wavefront generated by a point through the strip. The wavefront is curved because the source is a point.

When there is a point source, the shape of the wave front resembles an arrow. This automaton uses 4 neighbours system for propagation in 2D instead of 8 neighbours. This is the reason for the arrow-like shape instead of having a curve wave front.

Figure 4.7 shows the propagation of a planar front wave. The beat was originated in the left border of the strip.

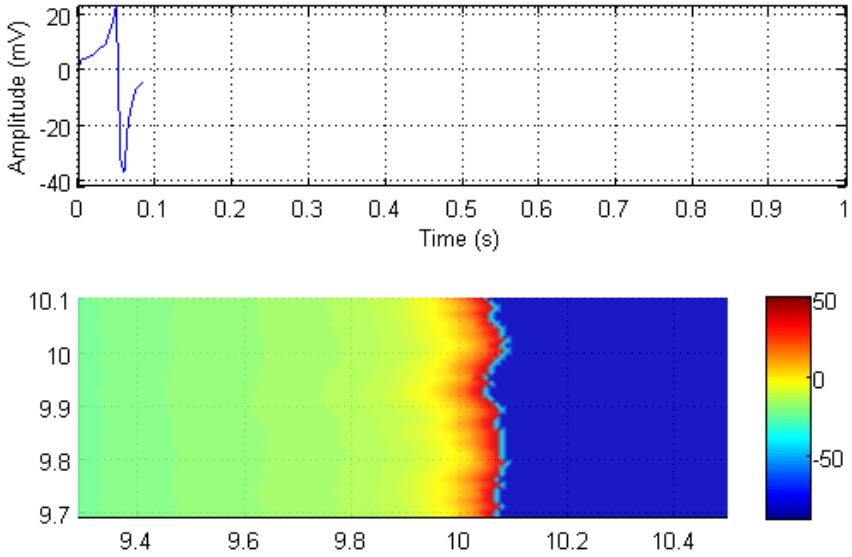

Figure 4.7. Propagation on a strip with a front wave source. The upper part shows the EGM recorded by the electrode and the lower part shows the propagation of the wavefront generated by a planar front through the strip. The wavefront is planar because the source is a line.

This case also behaves as expected. The wave front is a planar as it is supposed to be. The irregularities in the planar wave front are due to the probabilistic component of the automaton.

The same simulations are made for a cross to observe the behaviour when a bifurcation is reached. Figure 4.8 shows the propagation when the excitation starts in the point with coordinate (9.5, 9.9). Figure 4.9 shows the propagation when the whole left side of the cross is excited.

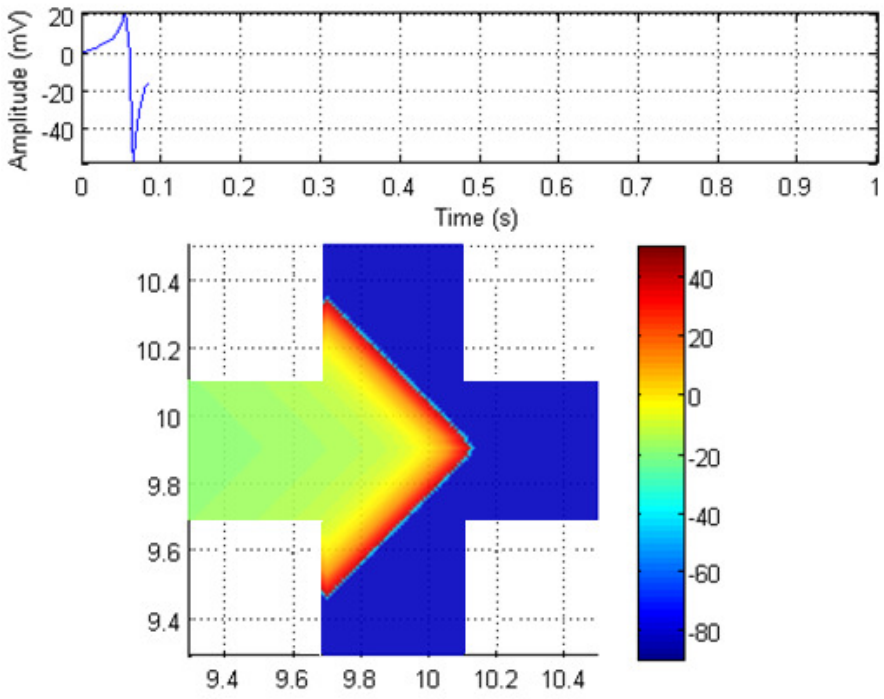

Figure 4.8. Propagation on a cross with a point source. The upper part shows the EGM recorded by the electrode and the lower part shows the propagation of the wavefront generated by a point through the cross. The wavefront is like an arrow because the source is a point.

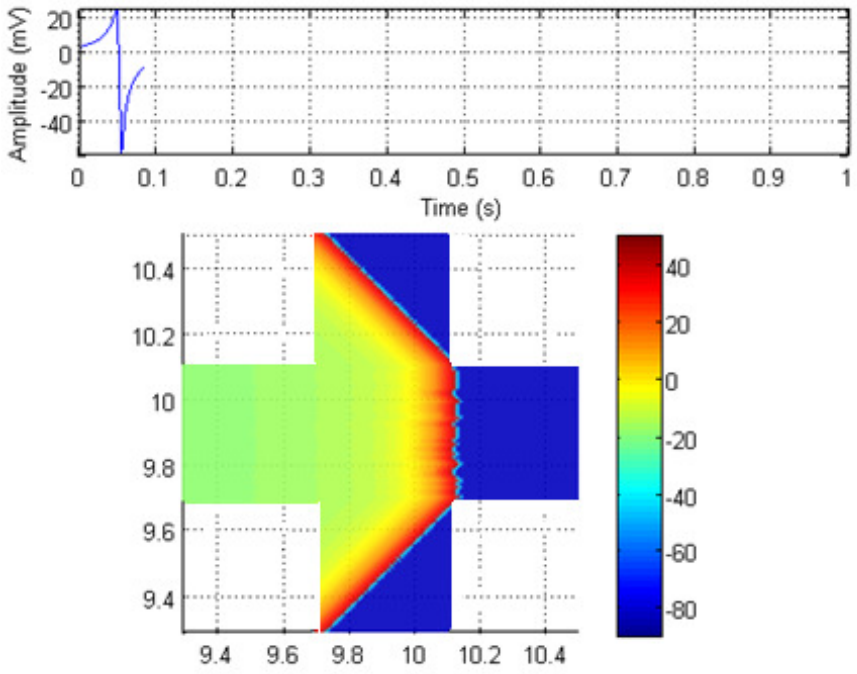

Figure 4.9. Propagation on a cross with a front wave source. The upper part shows the EGM recorded by the electrode and the lower part shows the propagation of the wavefront generated by a planar front through the cross. The wavefront is planar because the source is a line.

We can see similar behaviour as in the previous cases. Figure 4.8 shows the arrow shape behaviour of the front wave and how it spreads in the bifurcation. With the planar excitation in the left side of the cross, the behaviour is the expected. When this planar wave front reaches a bifurcation (Figure 4.9), it will become point source for the propagation in the bifurcation.

4.3 Simulations with different action potentials

These simulations are made on the same conditions but just changing the action potentials from ones simulation to another. The actions potentials are from ventricular, atrial and sinoatrial node cells shown in Fig 3.9.

4.3.1 Simulation with a strip

First, the behaviour is checked in the same strip model described in section 3.8. The electrode picked to analyze the EGM in the three cases is electrode 29 which is underneath the strip. This is done to be able to observe a better signal and to compare the results between the different cases. The results for the three cases are shown in Figure 4.10.

The differences between the EGM in the ventricular and atria cells are noticeable in the T wave. The complex PQRS does not change from one signal to the other (Fig. 4.10 a) and b)). Figure 3.9 shows that the upstroke of the action potential is very similar in both cases. They differ in the repolarization phase. The ventricular action potential has plateau which is not shown in the atria action potential. This plateau with the steeper repolarization curve increases the amplitude of the T wave in the repolarization. In the atria case, the repolarization is done smoothly with a more gradual slope which creates a smaller T wave.

When looking at Figure 4.10 c), the difference in the shape of the EGM of the sinoatrial node cells with respect to the ventricular myocytes is remarkable. There is a difference both in the PQRS complex and in the T wave. The PQRS has a longer duration because the upstroke of the action potential is not as steep. It takes longer to depolarize the cell and this is seen in the PQRS. The lack of plateau phase makes the T wave appear right after the point S.

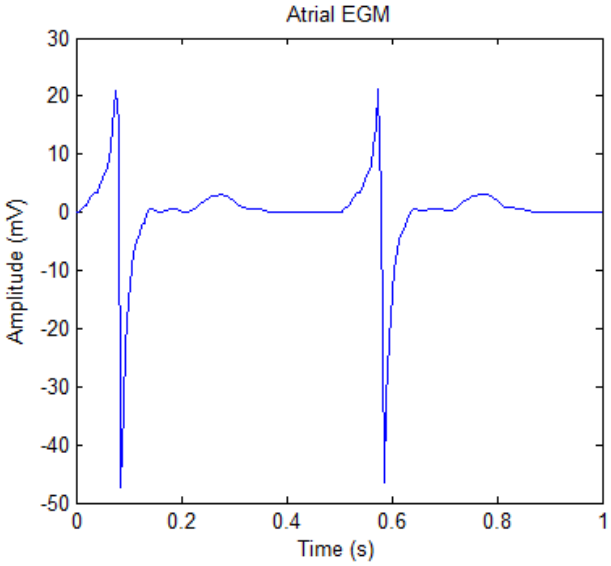

a)

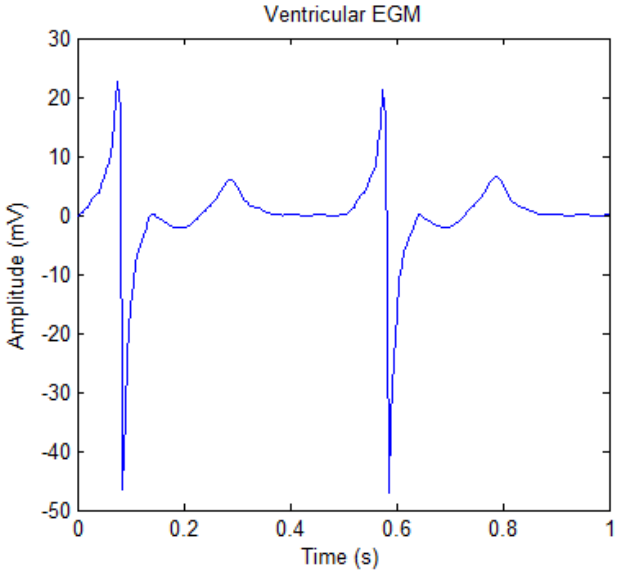

b)

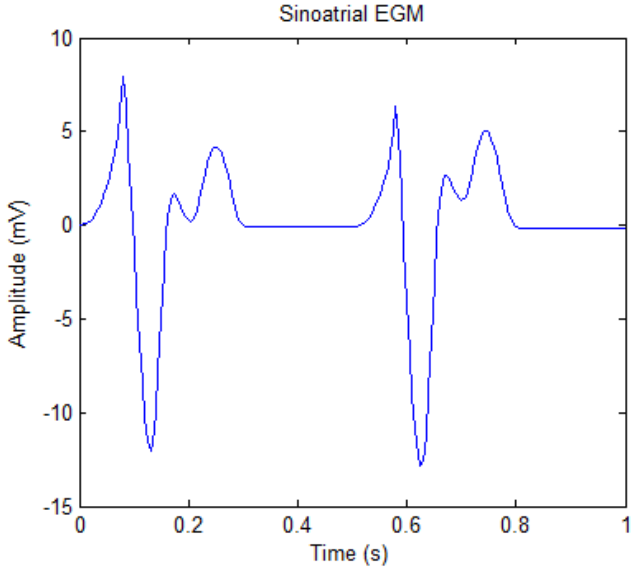

c)

Figure 4.10. EGM for the different types of cells generated in the simulation with a stripe of tissue: a) atrial, b) ventricular and c) sinoatrial node.

To be able to compare the changes of the EGM in better conditions, the amplitude of the three EGM were normalized having 1 as maximum value (Figure 4.11).

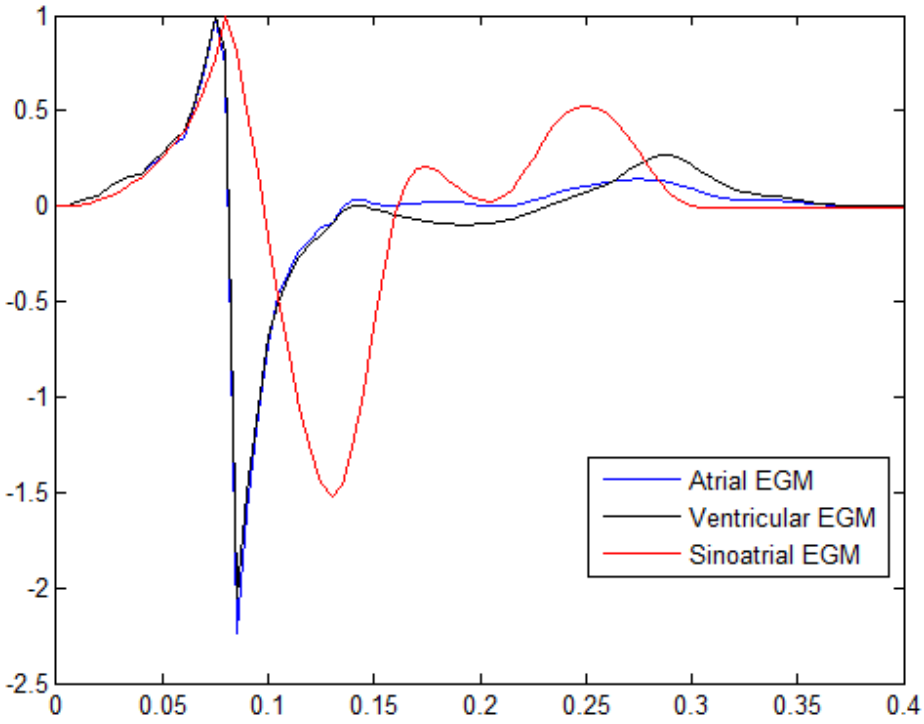

Figure 4.11. Comparison of the shape of EGM for the different types of cells when the signal has been normalized.

4.3.2 Simulation with the cell model

The next set of simulations is done in the model obtained from the cell culture. The EGM shown are coming from the electrode behind the cell culture, in this case, electrode 53 (Figure 4.12).

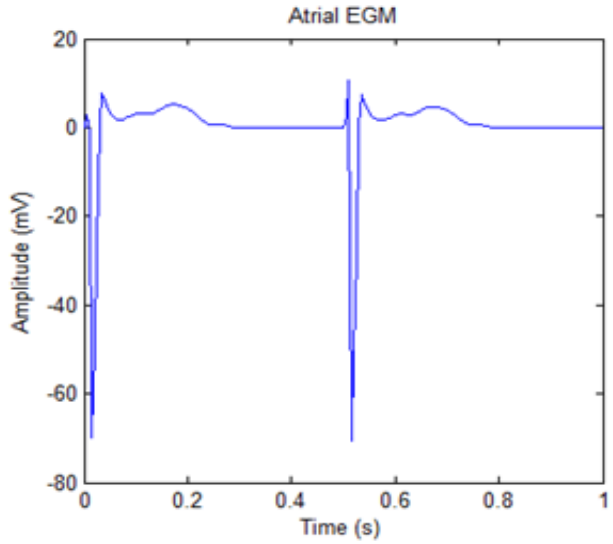

a)

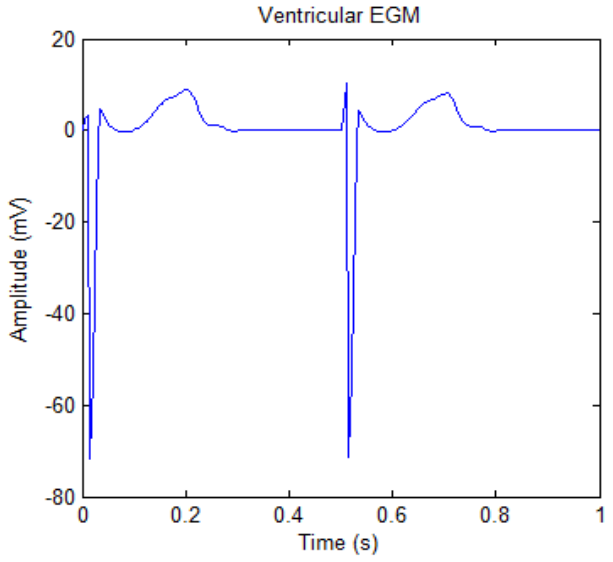

b)

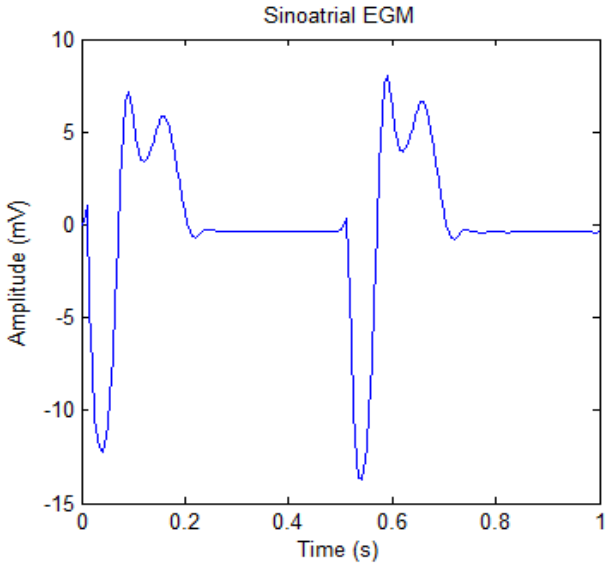

c)

Figure 4.12. EGM for the different types of cells generated in the simulation of the cell culture: a) atrial, b) ventricular and c) sinoatrial node.

To be able to discern better the changes in the shape of the EGM, the amplitude of the three EGM were normalized having 1 as maximum value. Now, the changes that are observed in Figure 4.13 are only due to changes in the shape of the signal and not due to changes in the maximum value of the action potential.

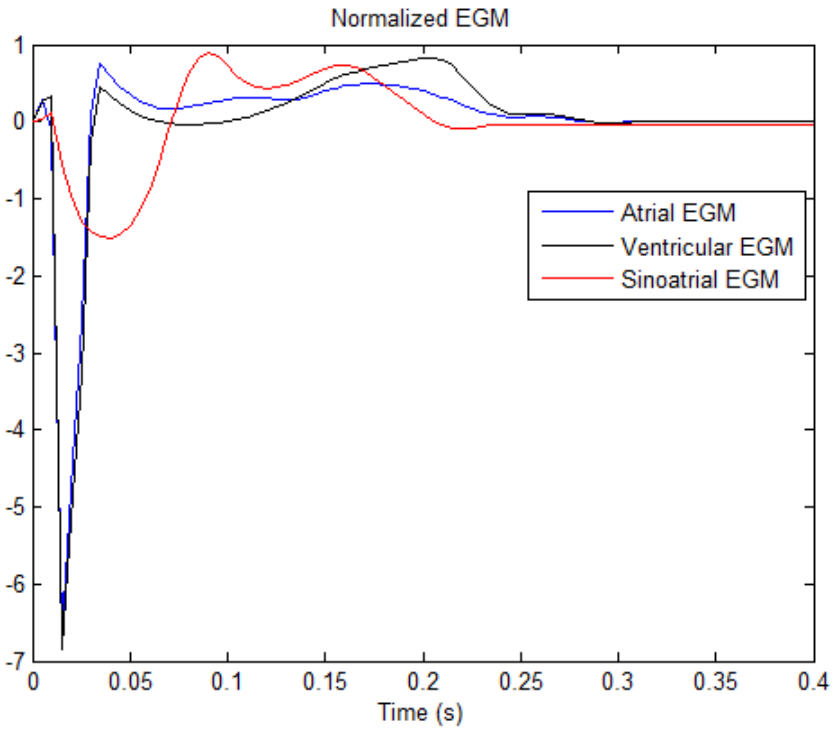

Figure 4.13. Comparison of the shape of EGM for the different types of cells when the signal has been normalized.

As it was seen in the previous case, the differences between the atrial and ventricular cases can be observed in the T wave. Figure 4.12 a) and b) show a difference in the amplitude of the T wave, as the one shown in the section 4.3.1. The differences in the shape of the PQRS complex are not noticeable. The amplitude of the signal is slightly different but it is due to the amplitude difference between the action potentials of atrial and ventricular cells (Figure 3.5).

Figure 4.12 c) shows the EGM recorded for the SA cell. The shape differs from the shape of the EGM of the atrial and ventricular cells (Figure 4.12 a) and b)). The PQRS complex has also longer duration due to the smaller slope in the upstroke of the action potential as shown in section 4.3.1. The change from downward to upward slope in the action potential due to the lack of resting voltage in the sinoatrial cells causes the changes of polarity in the T wave.

In Figure 4.13, the signals are normalized to be able to look at the differences in morphology without taking into account the changes in the amplitude due to the difference in the maximum amplitude of the action potentials. It is clearly seen that the sinoatrial EGM has a very different shape. The difference in the T wave between atrial and ventricular EGM is clearly seen in the normalized signal while the PQRS complex is almost identical in both cases.

4.3.3 Simulation of EGM with the cell model after the amplifier

The last set of simulations is done including the amplifier and the noise in the measurements to find a more realistic simulation.

The filter described in section 3.2.4 with the gain of 1100 is applied to the signals from the previous section to see how the cut off frequencies affect the signal. When they are normalized, Figure 4.14 is obtained.

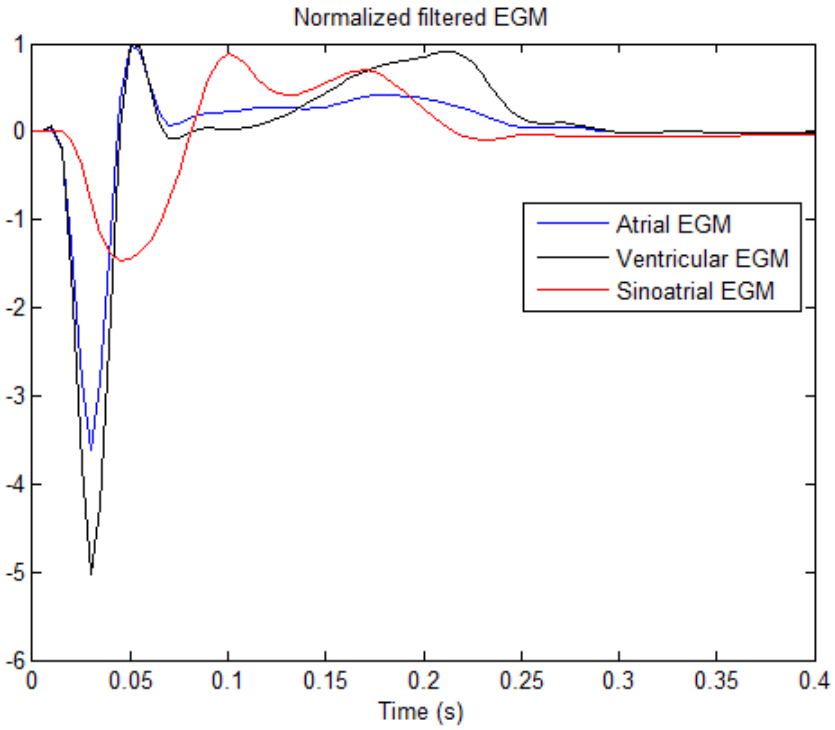

Figure 4.14. Comparison of the shape of EGM for the different types of cells which have been amplified when the signal has been normalized.

Comparing Figure 4.13 with Figure 4.14, the sharp changes in the signals are smoother because the amplifier removes the high frequencies of the signals which cause these sharp edges. In the other hand, the amplifier does not remove the features in the T wave which were differentiating the EGMs. Therefore, after the amplifier, the signal does not change the shape significantly and the same reasoning as before can be applied.

As it was said before, the real measurements systems introduce noise to the recorded signal. To simulate this situation, a random noise with amplitude of 20% of the maximum amplitude of the signal is added to the ideal signal from previous section. Figure 4.15 shows the new EGMs.

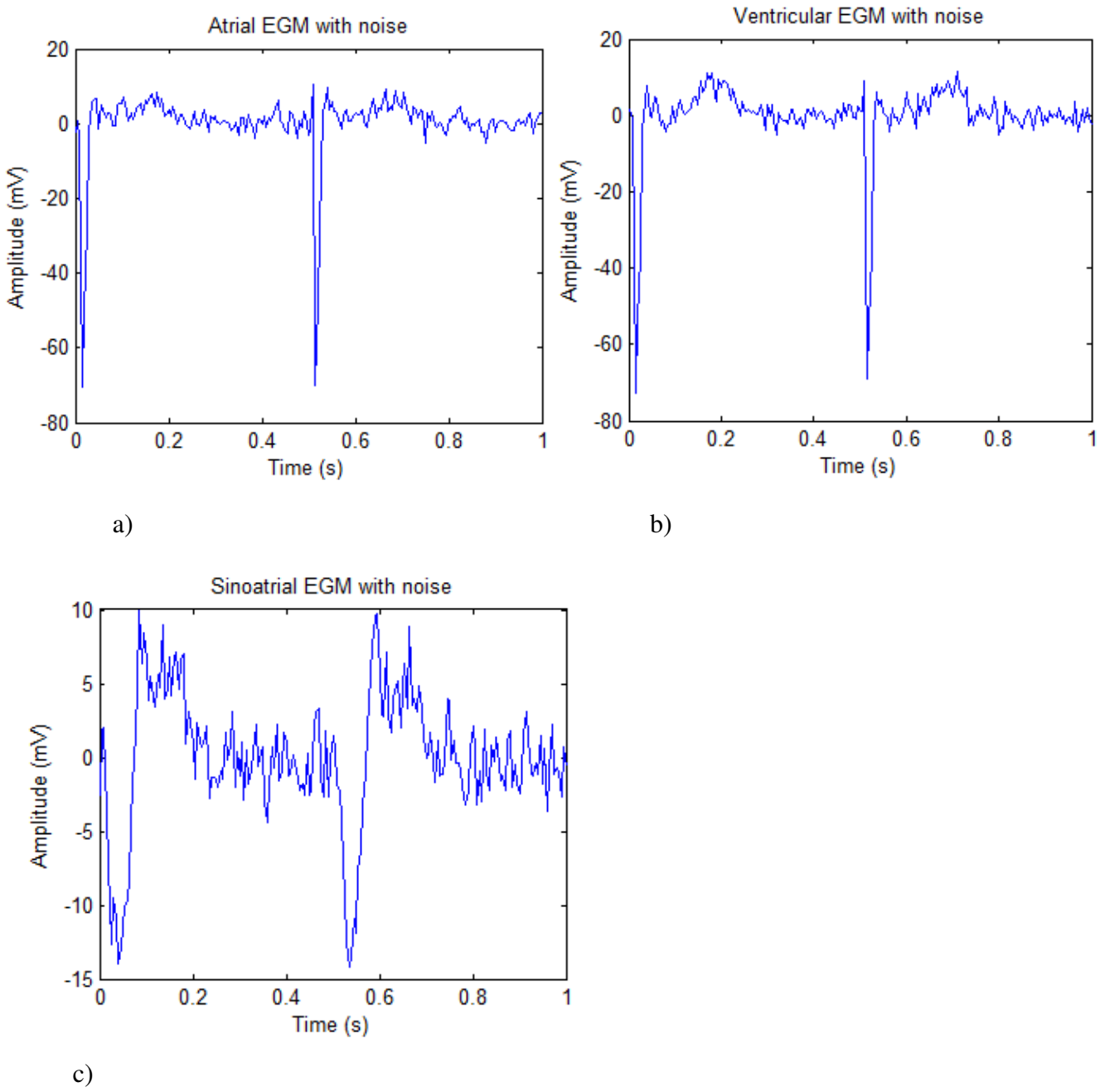

Figure 4.15. EGM for the different types of cells: a) atrial, b) ventricular and c) sinoatrial node with a noise amplitude of 20% of the signal amplitude.

Figure 4.16 shows the normalized EGMs are when the amplifier is applied to the noisy signals.

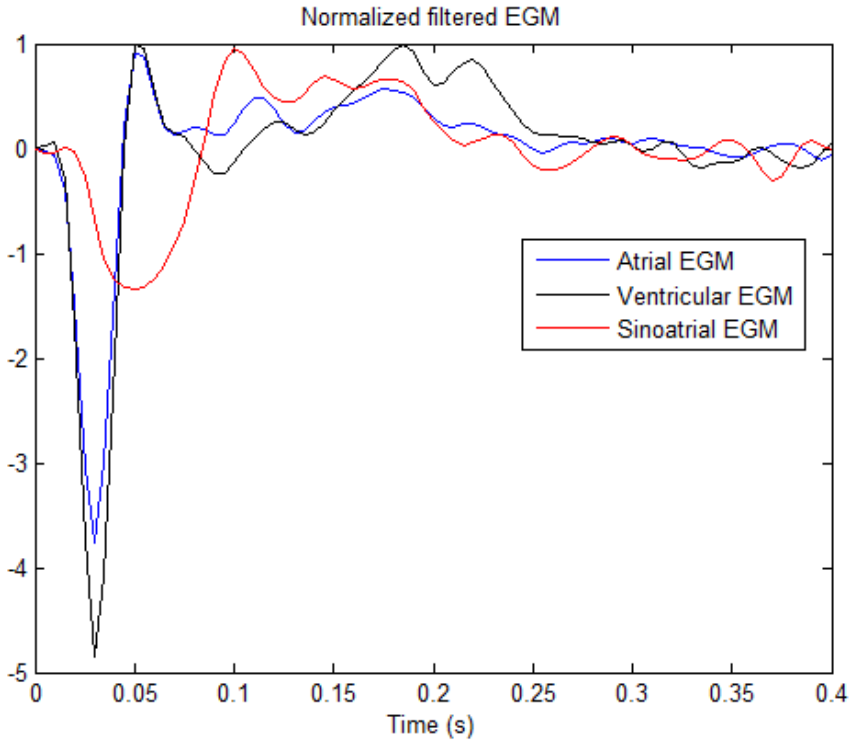

Figure 4.16. Comparison of the shape of EGM for the noisy EGM when they have been amplified and normalized.

When there is noise in the signal, the differences between different types of cells are not that easy to see. Figure 4.15 shows the original signals with the noise which is proportional to the amplitude of the signals. Figure 4.16 shows the signal at the output of the amplifier. The signals have been distorted because of the noise which is not completely removed but there are still some differences in the features used before. The sinoatrial cells still show a different morphology in the EGM. While the atrial and ventricular cells are more difficult to differentiate due to the noise effect. The amplitude of the T wave is still bigger in the ventricular EGM, but it is not that easy to be discerned due to the noise effects.

5 Discussion

This work has shown that it is possible to notice a difference in the EGM measured by the MEA between different types of cardiomyocytes. The difference in the APD of each type of cardiomyocytes is big enough to be noticeable in the EGM. The differences between atrial and ventricular are not very discernible, but the sinoatrial recordings differ significantly from the others.

On the other hand, there are limitations in the method still. This is the starting point for a complete study in this subject. There are several issues which have not been addressed in this project. The first point is the inhomogeneity of the cell cultures. In this thesis, homogeneous cell cultures have been simulated. But in real experiments, there are heterogeneous cell cultures. This kind of heterogeneous cell cultures should be simulated to see which ratio of different cell types could be differentiated. It may be possible that some kind of heterogeneous cell cultures produce the same EGM as homogeneous cell cultures in the simulations because the electrodes only reflects the activity of a small region of the cell culture. To compare two cell cultures as a whole, the EGM from the whole set of electrodes should be compared. Each electrode will have the information of a small region. If we compare just the information from one electrode the comparison will be local, to make a global comparison of the whole cell culture, all the electrodes have to be taken into account.

Another thing to take into account is the maturity phase of the cells. There is the possibility of having cells in different phases of maturity in the same cell culture. This will alter the EGM but it has to be study in which way it would change it. To be able to simulate this behaviour, the APD for difference phases are needed. This implies an electrophysiological study of the cell at different stages. Once that the APD have been acquired for several stages of the atrial, ventricular and sinoatrial cardiomyocytes, new simulations of heterogeneous cell cultures could be done. This would help to observe if it is possible to discern the cells at different stages using the MEA recordings.

It requires a lot of research to make a complete study in the subject, but the preliminary results are positive. If it is possible to differentiate the cell types in the cell cultures just looking at the EGM, the benefits could be important for the stem cell research. It would be an easy way to verify which types of cells are included in the cell culture. It would be

possible to check how the cell culture behaves during the time and how the maturation process takes place. This could be a nice tool for everyday work in the laboratory. The main difference with patch clamp would be that looking at all the electrodes of the MEA, a whole picture of the cell culture can be seen. On the other hand, patch clamp just analyzes a single cell.

Therefore, this is the first step of a research which could be used to develop a very useful tool. But all these suppositions have to be confirmed in further research in the laboratory.

6 Conclusion

The first result of this work is the computer model to simulate the electrical behaviour of the cell cultures. It was possible to generate the FDM model of the cell culture even though that the solver that it was used was not planned to work with such small resolution.

In section 4.1, it is explained that is not possible to use the same set of lead field for a specific MEA without taking into account the cell culture that is on it. It would have been an advantage just to calculate on set of lead fields for a specific MEA structure and use it for different cell cultures. This is not possible because even though the cell cultures are small, their conductivities change the value of the lead fields. Therefore the lead fields should be calculated for each different cell culture geometry.

The functionality of the cellular automata is proof in section 4.2. It behaves as expected in known geometries as strip and cross. Therefore the first objective of this thesis, which was to create a functional cellular automaton, was achieved.

The second objective was also achieved. The results confirm the hypothesis of classifying the types of cells just looking at the measurements without having prior information about them even with some noise. The differences between atrial and ventricular cells are not that easy to see due to the small differences in their action potentials. But sinoatrial cells are easily classified because their measured EGM are completely different from the contractile cells.

These results have been obtained with a computer model in which all the cells were ideal and from the same kind. There are many factors to be studied to extrapolate these results to in vitro measurements. The cells are derived from the stem cells and when they are measured, it is not known if they are fully mature or not. If they are not fully mature, the action potential will not have the same curves as the ones shown in this thesis. In the differentiation process, several types of cells are grown in the same cell culture. Therefore, the measured signals will not have the same shape as the ones shown in the thesis. But with some research, it could be see if it is possible to differentiate them when they are mostly of one type.

7 Bibliography

1. Caspi, O., Huber, I., Kehat, I., Habib, M., Arbel, G., Gepstein, A., Yankelson, L., Aronson, D., Beyar, R., Gepstein, L., Transplantation of human embryonic stem cell-derived cardiomyocytes improves myocardial performance in infarcted rat hearts., J Am Coll Cardiol 50 (2007), 1884-1893.

2. Takahashi K, et al., Induction of Pluripotent Stem Cells from Adult Human Fibroblasts by Defined Factors . Cell. 2007 Nov 30;131(5):861-72.

3. Yu J, Vodyanik MA, et al., Induced Pluripotent Stem Cell Lines Derived from Human Somatic Cells. Science. 2007 Dec 21;318(5858):1917-20.

4. Malmivuo J.A., Plonsey R. 1995. Bioelectromagnetism. Principles and Applications of Bioelectric and Biomagnetic Fields, Oxford University Press,

5. Beeler GW, Reuter H., Reconstruction of the action potential of ventricular myocardial fibers. J Physiol 1977, 268: 177-210.

6. Luo CH, Rudy Y., A dynamic model of the cardiac ventricular action potential. I. Simulations of ionic currents and concentration changes. 1994, Circ Res 74: 1071-1096.

7. Luo CH, Rudy Y., A model of the ventricular cardiac action potential, depolarization, repolarization and their interaction. 1991, Circ Res 68: 1501-1526.

8. Fenton FH, Karma A. , Vortex dynamics in three-dimensional continuous myocardium. Filament instability and fibrillation. 1998, Chaos 8: 20-47.

9. FitzHugh, R. A., Impulses and physiological states in theoretical models of nerve membran. 1961, Biophys J, 1: 445–466 .

10. McCulloch, J. M. Rogers and A. D., A collocation-Galerkin finite element model of cardiac action potential propagation. 1994, IEEE Transactions on Biomedical Engineering, vol. 41, 8, 743–757.

11. Moe G. K., Rheinboldt W. C., and Abildskov J. A.., A computer model of atrial fibrillation. 1964, Am. Heart J, 67, 200–220.

12. Werner C. D., Sachse F. B., andDössel O.., Applications of the Visible Man dataset in electrocardiology: Simulation of the electrical excitation propagation. 1998, Proc. Second Users Conference of the National Library of Medicine's Visible Human Project,69–79.

13. Alonso Atienza F, Requena Carrión J, García Alberola A, Rojo Álvarez JL, Sánchez Muñoz JJ, Martínez Sánchez J, et al., Desarrollo de un modelo probabilístico de la actividad eléctrica cardíaca basado en un autómata celular. 2005, Rev Esp Cardiol., págs. 58:41-7.

14. Marieb E.N., 2006, Essentials of Human Anatomy and Physiology. s.l. : Pearson Benjamin Cummings.

15. Sherwood L., 2007, Human Physiology. From Cells to Systems. : Thomson Brooks/Cole,.

16. Berne R.M., Levy M.N. 1997, Cardiovascular Physiology. : Mosby

17. Romero L., Ferrero J.M., Saiz F.J. et al., Effects of Acute Ischemia on the Restitution Curves of Myocardial Tissue: A Simulation Study. Computers on Cardiology 2004, 525-528.

18. Ogden., D.C. 1994, Microelectrode techniques, The Plymouth workshop handbook.2nd Edition: Company of Biologists,Cambridge, UK.

19. Reppel, M., Pillekamp, F., Lu, Z. J., Halbach, M., Brockmeier, K., Fleischmann, B. K., and Hescheler, J. Microelectrode arrays: A new tool to measure embryonic heart activity. (2004) Journal of Electrocardiology 37, 104-109.

20. Cole, K. S. Dynamic electrical characteristics of the squid axon membrane. (1949). Arch. Sci. Physiol.3, 253-258.

21. Hodgkin, A. L., Huxley, A. F. and Katz, B., Measurement of current-voltage relations in the membrane of the giant axon of Loligo. (1952). J. Physiol., Lond. 116, 424-448.

22. Neher, E. and Sakmann, B., Single channel currents recorded from membrane of denervated frog muscle fibres. (1976).Nature, Lond. 260, 799-802.

23. Neher, E., Sakmann, B. and Steinbach, J. H., The extracellular patch clamp: a method for resolving currents through individual open channels in biological membranes. (1978).Pflügers Arch. 375, 219-228.

24. Hamill, O.P., Marty, A., Neher, E., Sakmann, B. and Sigwortg, F. J. , Improved patchclamp techniques for high-resolution current recording from cells and cell-free membrane patches. (1981). Pflügers Arch. 391, 85-100.

25. Thomas CA, Springer PA, Loeb GE, Berwald-Netter Y, Okun LM., A miniature microelectrode array to monitor the bioelectric activity of cultured cells. 1972. Exp Cell Res. 74: 61-66.

26. Gross GW, Rieske E, Kreutzberg GW, Meyer A ., A new fixed-array multimicroelectrode system designed for long-term monitoring of extracellular single unit neuronal activity in vitro. (l977).Neurosci. Lett. 6: 101-105.

27. Meyer, T., Boven, K. H., Gunther, E., and Fejtl, M., Micro-electrode arrays in cardiac safety pharmacology: a novel tool to study QT interval prolongation. (2004).Drug Saf 27, 763-72.

28. Reppel, M., Igelmund, P., Egert, U., Juchelka, F., Hescheler, J., and Drobinskaya, I., Effect of cardioactive drugs on action potential generation and propagation in embryonic stem cell-derived cardiomyocytes. (2007).Cell Physiol Biochem 19, 213-24.

29. Pfannkuche, K., Liang, H., Hannes, T., Xi, J., Fatima, A., Nguemo, F., Matzkies, M., Wernig, M., Jaenisch, R., Pillekamp, F., Halbach, M., Schunkert, H., Saric, T., Hescheler, J., and Reppel, M. (2009). Cardiac myocytes derived from murine reprogrammed fi.

30. Pekkanen-Mattila, M., Kerkela, E., Tanskanen, J. M., Pietila, M., Pelto-Huikko, M., Hyttinen, J., Skottman, H., Suuronen, R., and Aalto-Setala, K. Substantial variation in the cardiac differentiation of human embryonic stem cell lines derived and propagated under the same conditions-a comparison of multiple cell lines. (2009). Ann Med, 1-15.

31. Binah, O., Dolnikov, K., Sadan, O., Shilkrut, M., Zeevi-Levin, N., Amit, M., Danon, A., and Itskovitz-Eldor, J. (2007). Functional and developmental properties of human

embryonic stem cells-derived cardiomyocytes. Journal of Electrocardiology 40, S192-S19.

32. Zwi, L., Caspi, O., Arbel, G., Huber, I., Gepstein, A., Park, I.-H., and Gepstein, L. (2009). Cardiomyocyte Differentiation of Human Induced Pluripotent Stem Cells. Circulation, CIRCULATIONAHA.109.868885.

33. Marshak D.R. & Gardner, R.L. 2001, Stem Cell Biology.

34. Liebert. M.A., TISSUE ENGINEERING: Part B, Volume 14, Number 1, pp.53 - 57. 2008.

35. V. Gmyr, J. Kerr-Conte, S. Belaich, B. Vandewalle, E. Leteurtre, M. C. Vantyghem, Adult human cytokeratin 19-positive cells reexpress insulin promoter factor 1 in vitro: further evidence for pluripotent pancreatic stem cells in humans. Diabetes 2000, 49, 1671-1680.

36. Hierlihy, A.M., Seale, P., Lobe, C.G., Rudnicki, M.A., and Megeney, L.A., The post-natal heart contains a myocardial stem cell population. : 2002, FEBS Lett 530, 239

37. Martin, C.M., Meeson, A.P., Robertson, S.M., Hawke, T.J., Richardson, J.A., Bates, S., Goetsch, S.C., Gallardo, T.D., and Garry, D.J, Persistent expression of the ATP-binding cassette transporter, Abcg2, identifies cardiac SP cells in the developing and adult heart. : Dev Biol 265, 262, 2004.

38. Kastenberg Z.J., Odorico J.S., Alternative sources of pluripotency: science, ethics, and stem cells. s.l. : (2008) Transplantation Reviews, 22 (3), pp. 215-222. .

39. Genetic Science Learning Center (2010, May 28) Creating Stem Cells for Research. Learn.Genetics. Retrieved August 16, 2010, from http://learn.genetics.utah.edu/content/tech/stemcells/sccreate/

40. Nombela C., Células madre: encrucijadas biológicas para la medicina: del tronco embrionario a la regeneración adulta. s.l. : EDAF, 2007.

41. Kruse, C., Danner, S. and Rapoport, D., Current Stem Cell Technology: Limitations and Realistic Expectations. (2008), Engineering in Life Sciences, 8: 13–18.

42. Models of cardiac cells. Refered on 10 July 2010, http://www.scholarpedia.org/article/Models_of_cardiac_cel.

43. Hodgkin L, Huxley AF. , A quantitative description of membrane currents and its application to conduction and excitation in nerve. 1952, J Physiol 117: 500-544.

44. Sachse, F.B. Computational cardiology modelling of anatomy, electrophysiology and mechanics.

45. Cabo C, Boyden PA., Electrical remodeling of the epicardial border zone in the canine infracted heart: a computational analysis. 2003, Am J Physiol 284: H372-H384.

46. Hund TJ, Rudy Y. , Rate dependence and regulation of action potential and calcium transient in a canine cardiac ventricular cell model. 2004, Circulation 110: 3168-3178.

47. Greenstein JL, Winslow RL., An integrative model of the cardiac ventricular myocytes incorporating local control of Ca2+ release. 2002, Biophys J 83 H2918-H2945.

48. Mahajan A, Shiferaw Y, Sato D, Baher A, Olcese R, Xie LH, Yan MJ, Chen PS, Restrepo JG, Karma A, Garfinkel A, Qu Z, Weiss JN. , A rabbit ventricular action potential model replicating cardiac dynamics at rapid heart rates. 1998, Biophys J 94: 392-410.

49. Courtemanche M, Ramirez RJ, Nattel S., Ionic mechanisms underlying human atrial action potential properties: insights from a mathematical model. 1998, Am J Physiol 275: H301-H321.

50. Simitev RD, Biktashev VN., Conditions for propagation and block of excitation in an asymptotic model of atrial tissue. 2006, Biophys J 90: 2258-2269.

51. Priebe L, Beuckelmann DJ., Simulation study of cellular electric properties in heart failure. 1998, Circ Res 82: 1206-1223.

52. Bernus O, Wilders R, Zemlin CW, Verschelde H, Panfilov AV., A computationally efficient electrophysiological model of human ventricular cells. 2002, Am J Physiol 282: H2296-H2308.

53. Iyer V, Mazhari R, Winslow RL., A computational model of the human left-ventricular epicardial myocyte. 2004, Biophys J 87: 1507-1525.

54. Ten Tusscher KH, Noble D, Noble PJ, Panfilov AV, A model for human ventricular tissue, 2004, Am J Physiol 286: H1573-H1589.

55. Pullan A., M.L. Buist and L.K. Cheng. Mathematically modelling the electrical activity of the heart, World Scientific, 2005.

56. Rosenblueth, N. and Wiener, A., The mathematical formulation of the problem of conduction of impulses in a network of connected excitable elements specifically in cardiac muscle. 1946, Arch. Del. Instit. De Cardiologia De Mexico, 16, 205–265.

57. Vichniac, Gérard Y. , Simulating Physics with Cellular Automata. 1984, Physica 10D, 96-116.

58. Toffoli, Tommaso. ,Cellular Automata as an Alternative to (rather than an Approximation of Differential Equations in Modelling Physic. 1984, Physica 10D, 117-127.

59. Wei D. , Okazaki O., Harumi K., Harasawa E., and Hosak H., Comparative simulation of excitation and body surface electrocardiogram with isotropic and anisotropic computer heart models, Apr. 1995, IEEE Transactions on Biomedical Engineering vol. 42, no. 4, pp. 343–357

60. Vaisainen, J., Methods for Analysing the Sensitivities of Bioelectric Measurements, Tampere University of Technology, 2010

61. Arola, T., Lead Field based Simulation Tool for Dipolar Bioelectric Fields. Tampere University of Technology 2003

62. http://www.multichannelsystems.com/uploads/media/MEA.pdf.

63. http://www.multichannelsystems.com/uploads/tx_ttproducts/datasheet/MEA1060_02.pdf.

64. Takano, N., Reducion of ECG Leads and Equivalent Sources Using Orthogonalization and Clustering Techniques. Tampere University of Technology, 2002

8 Appendix

A. Radius of the half sensitivity area

Electrode 1 (mm)	Electrode 2 (mm)	Electrode 3 (mm)	Electrode 4 (mm)	Electrode 5 (mm)	Electrode 6 (mm)	Electrode 7 (mm)	Electrode 8 (mm)
0.03007	0.03006	0.02005	0.02004	0.02004	0.02000	0.02001	0.02000
Electrode 9 (mm)	Electrode 10 (mm)	Electrode 11 (mm)	Electrode 12 (mm)	Electrode 13 (mm)	Electrode 14 (mm)	Electrode 15 (mm)	Electrode 16 (mm)
0.03007	0.03006	0.03007	0.03007	0.03005	0.03001	0.02999	0.02000
Electrode 17 (mm)	Electrode 18 (mm)	Electrode 19 (mm)	Electrode 20 (mm)	Electrode 21 (mm)	Electrode 22 (mm)	Electrode 23 (mm)	Electrode 24 (mm)
0.03007	0.03006	0.03007	0.03007	0.03005	0.03001	0.02001	0.02000
Electrode 25 (mm)	Electrode 26 (mm)	Electrode 27 (mm)	Electrode 28 (mm)	Electrode 29 (mm)	Electrode 30 (mm)	Electrode 31 (mm)	Electrode 32 (mm)
0.03007	0.03006	0.03007	0.03007	0.02004	0.02000	0.02001	0.02000
Electrode 33 (mm)	Electrode 34 (mm)	Electrode 35 (mm)	Electrode 36 (mm)	Electrode 37 (mm)	Electrode 38 (mm)	Electrode 39 (mm)	Electrode 40 (mm)
0.03007	0.03006	0.03007	0.03007	0.03005	0.03001	0.02001	0.02000
Electrode 41 (mm)	Electrode 42 (mm)	Electrode 43 (mm)	Electrode 44 (mm)	Electrode 45 (mm)	Electrode 46 (mm)	Electrode 47 (mm)	Electrode 48 (mm)
0.03007	0.03006	0.02005	0.02005	0.04005	0.03001	0.02001	0.02000
Electrode 49 (mm)	Electrode 50 (mm)	Electrode 51 (mm)	Electrode 52 (mm)	Electrode 53 (mm)	Electrode 54 (mm)	Electrode 55 (mm)	Electrode 56 (mm)
0.03007	0.03006	0.02005	0.02005	0.07005	0.02999	0.02001	0.02000
Electrode 57 (mm)	Electrode 58 (mm)	Electrode 59 (mm)	Electrode 60 (mm)	Electrode 61 (mm)	Electrode 62 (mm)	Electrode 63 (mm)	Electrode 64 (mm)
0.03007	0.03006	0.03007	0.02005	0.02039	0.02000	0.02001	0.02000

B. Matlab code

- Calculation of the excitability taking into account the CV and the conductivity of neighbouring cells:

```
nodes_excitability=restitution_CV(index_rCV).*nodes_rest.*nodes_non_is
ch+restitution_CV_cond(index_rCV).*nodes_rest.*nodes_non_isch;

amount_excitation=sum((state_allnodes(nodes_neigh)==2).*conectivity+(s
tate_allnodes(nodes_neigh)==4).*conectivity,2);

p_exc=K*amount_excitation.*nodes_excitability;
```

- Probabilisitc component of the cellular automata:

```
change_rest=(rand(size(p_exc))<p_exc).*nodes_rest;
```

- Calculation of the DI taking into account the time of excitation:

```
index_rCV=ceil(1+(a-1)*trapmf((t-t_rep)*1000,[0 a 10000 10001]));

t_rep=t*changes_refractary+t_rep.*not(changes_refractary);%Time (exact
moment) when was at rest(when the repolarization started)

t_desp=t*changes_rest+t_desp.*not(changes_rest);%Time (exact moment)
when was at excited(when the depolarization started)

index_restitution_APD=ceil(1+(a-1)*trapmf(abs(t_desp-t_rep)*1000,[0 a
10000 10001]));%Calculate DI

rAPD=restitution_APD(index_restitution_APD).*changes_rest.*nodes_non_i
sch+rAPD.*not(changes_rest);
```

- Calculation of the impress current:

```
V = voltage_allnodes(nodes_heart);
dv_dx_heart=repmat(V,1,3)-voltage_allnodes(nodes_neigh(:,1:3));
current(:,:,index_frame)=dv_dx_heart.*conectivity(:,1:3);
```

- Calculation of the EGM:

```
EGM_lf(j) = sum( sum ( current(:,:,j).*Lead_field(:,5:7 )));
```

C. Lead field for the strip and the cross

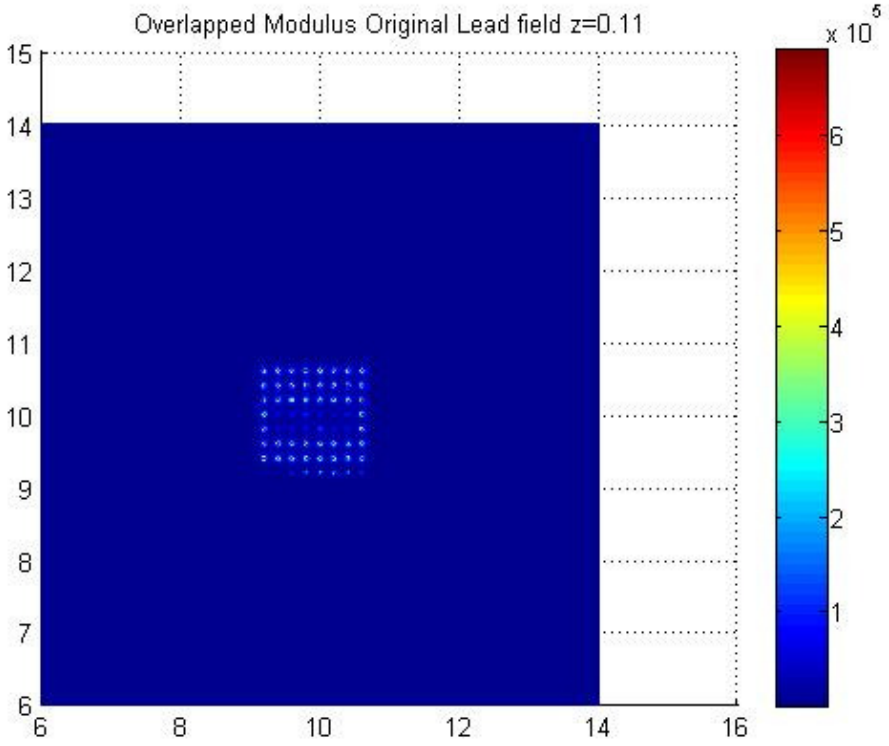

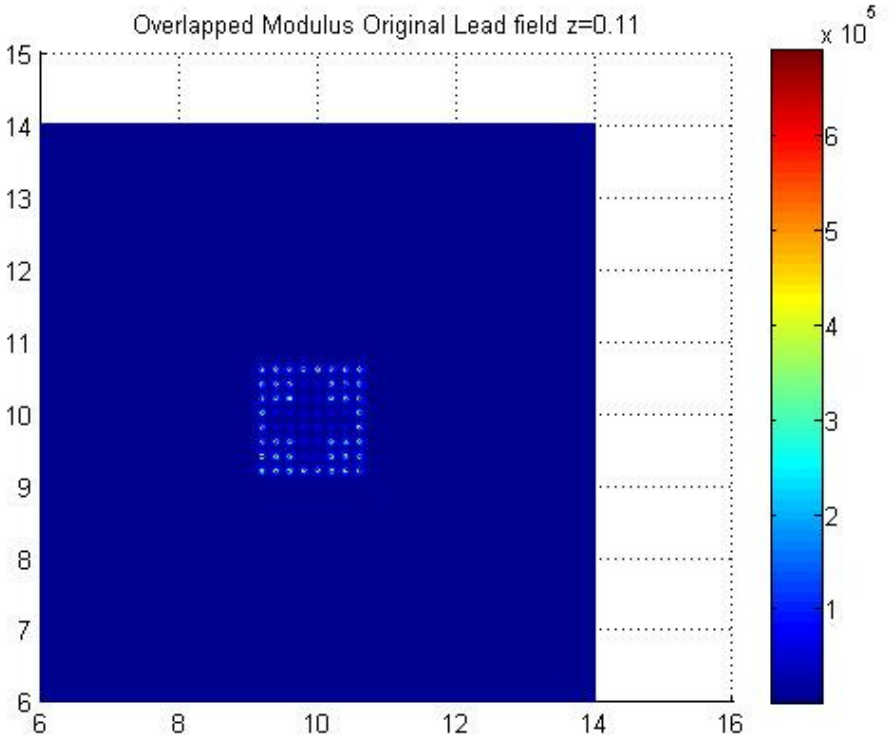

D. Simulations of the ventricular cell with the cell culture in the 64 electrodes

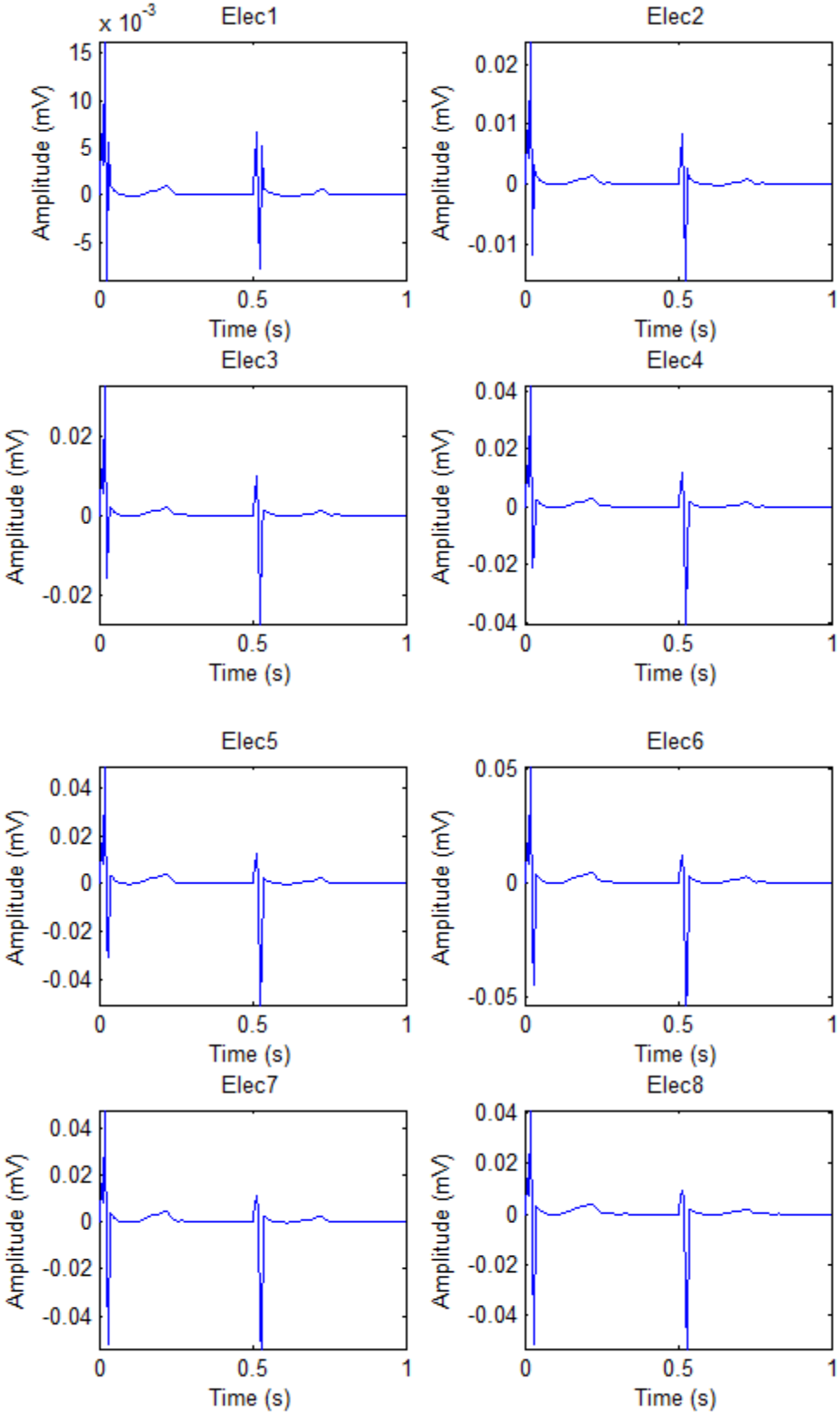

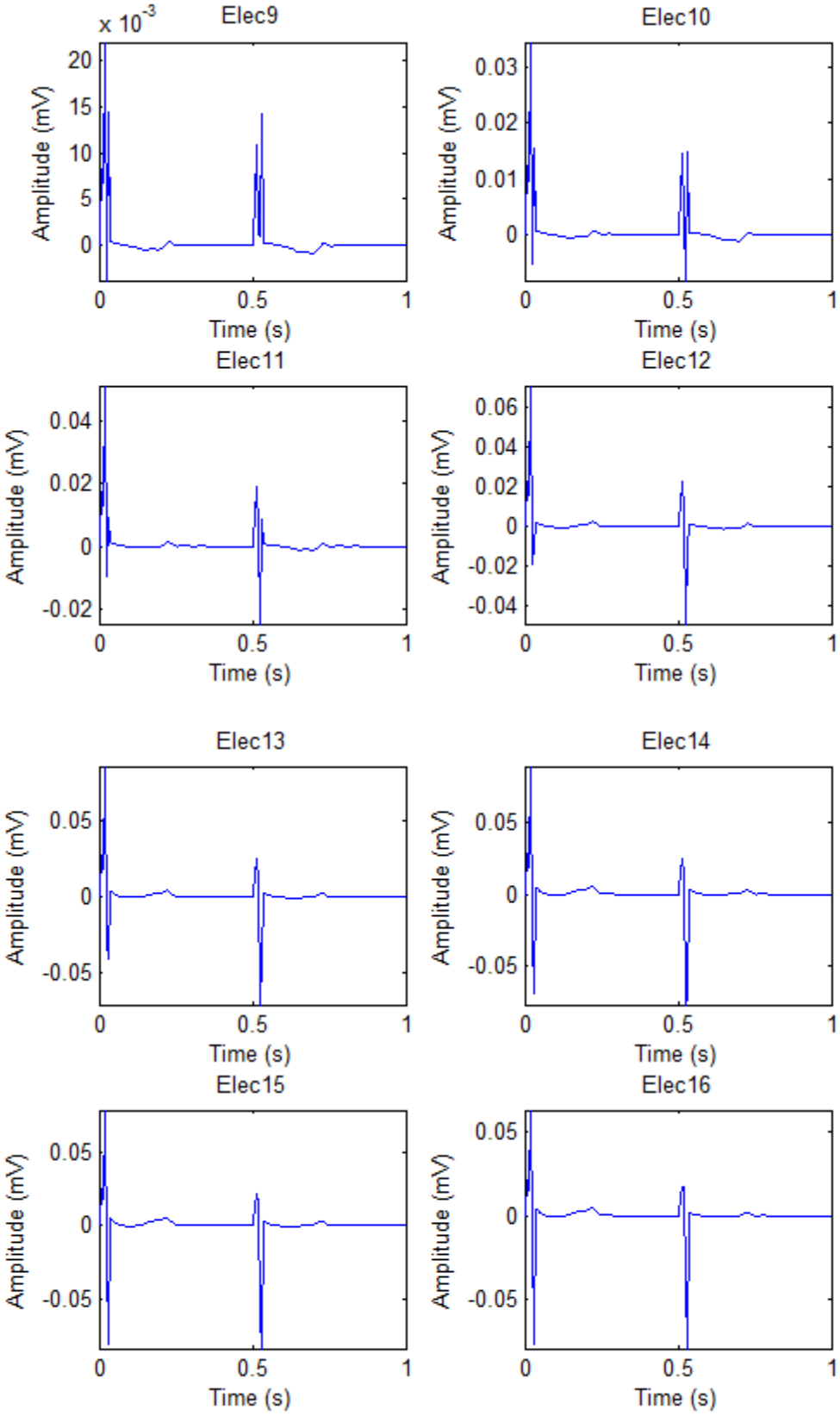
Elec9
x 10^-3
Amplitude (mV)
Time (s)
Elec10
Elec11
Elec12
Elec13
Elec14
Elec15
Elec16

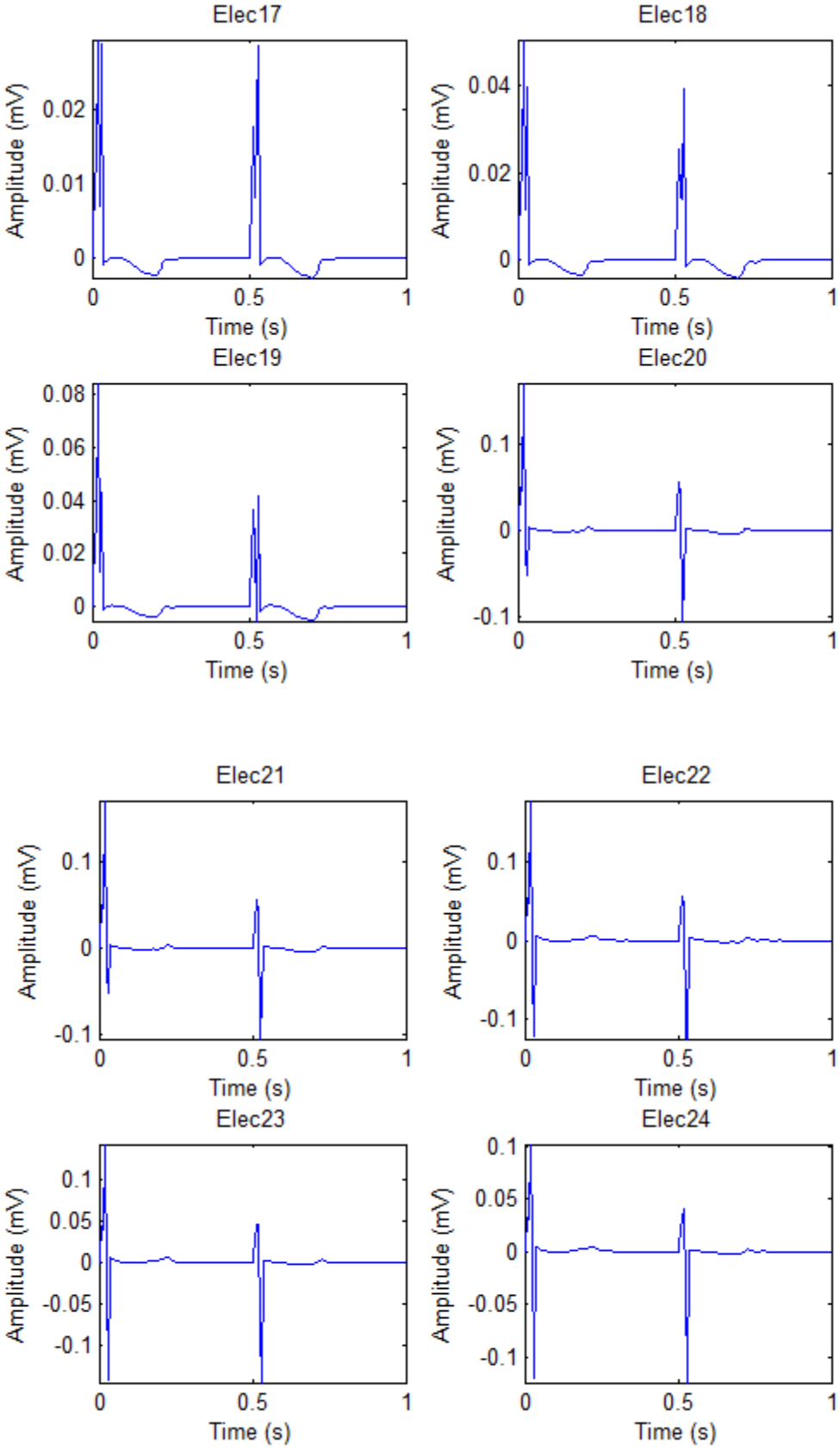
Elec17
Amplitude (mV)
0.02
0.01
0
0
0.5
1
Time (s)
Elec18
Amplitude (mV)
0.04
0.02
0
0
0.5
1
Time (s)
Elec19
Amplitude (mV)
0.08
0.06
0.04
0.02
0
0
0.5
1
Time (s)
Elec20
Amplitude (mV)
0.1
0
-0.1
0
0.5
1
Time (s)
Elec21
Amplitude (mV)
0.1
0
-0.1
0
0.5
1
Time (s)
Elec22
Amplitude (mV)
0.1
0
-0.1
0
0.5
1
Time (s)
Elec23
Amplitude (mV)
0.1
0.05
0
-0.05
-0.1
0
0.5
1
Time (s)
Elec24
Amplitude (mV)
0.1
0.05
0
-0.05
-0.1
0
0.5
1
Time (s)

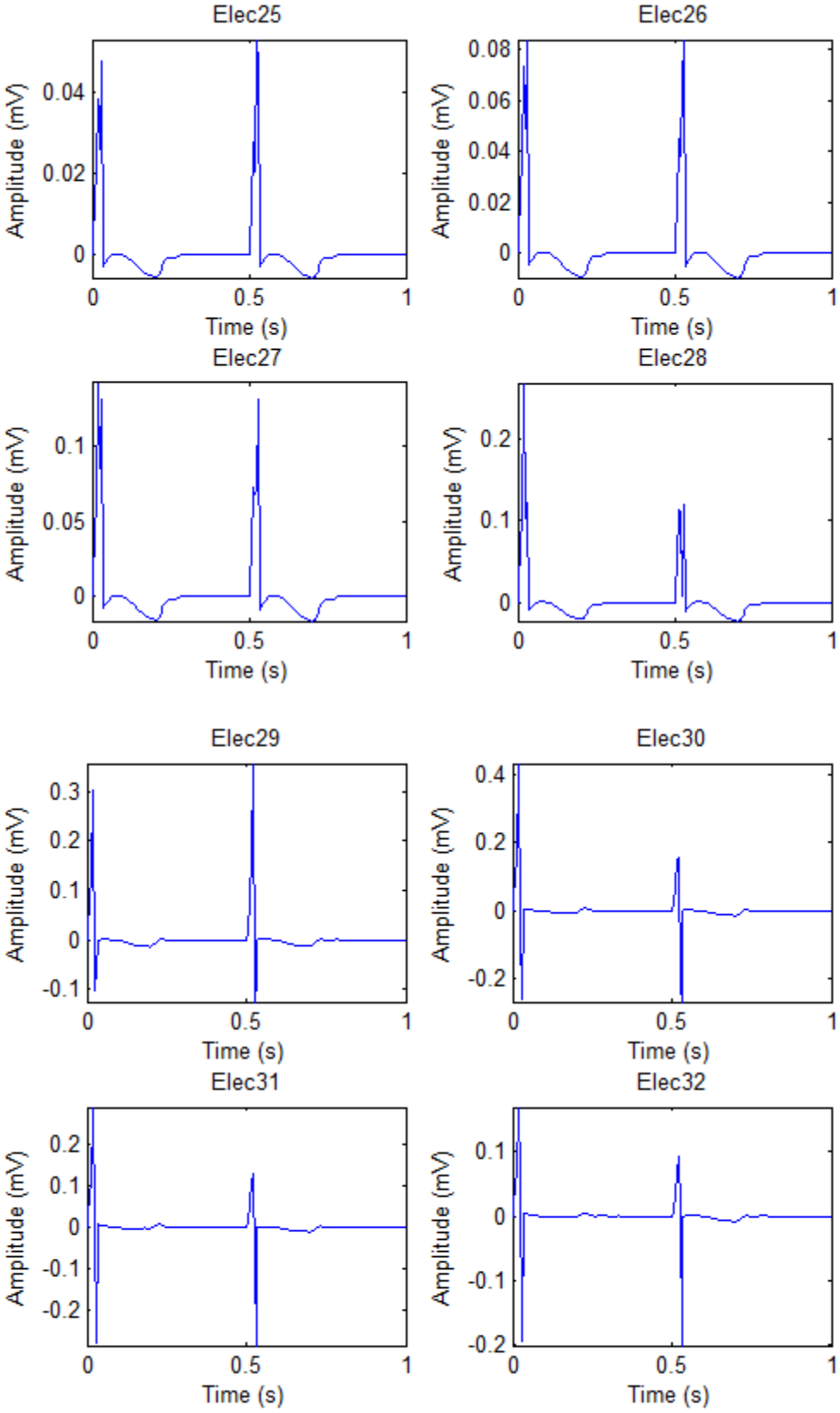
Elec25
Amplitude (mV)
0.04
0.02
0
0
0.5
1
Time (s)
Elec26
Amplitude (mV)
0.08
0.06
0.04
0.02
0
0
0.5
1
Time (s)
Elec27
Amplitude (mV)
0.1
0.05
0
0
0.5
1
Time (s)
Elec28
Amplitude (mV)
0.2
0.1
0
0
0.5
1
Time (s)
Elec29
Amplitude (mV)
0.3
0.2
0.1
0
-0.1
0
0.5
1
Time (s)
Elec30
Amplitude (mV)
0.4
0.2
0
-0.2
0
0.5
1
Time (s)
Elec31
Amplitude (mV)
0.2
0.1
0
-0.1
-0.2
0
0.5
1
Time (s)
Elec32
Amplitude (mV)
0.1
0
-0.1
-0.2
0
0.5
1
Time (s)

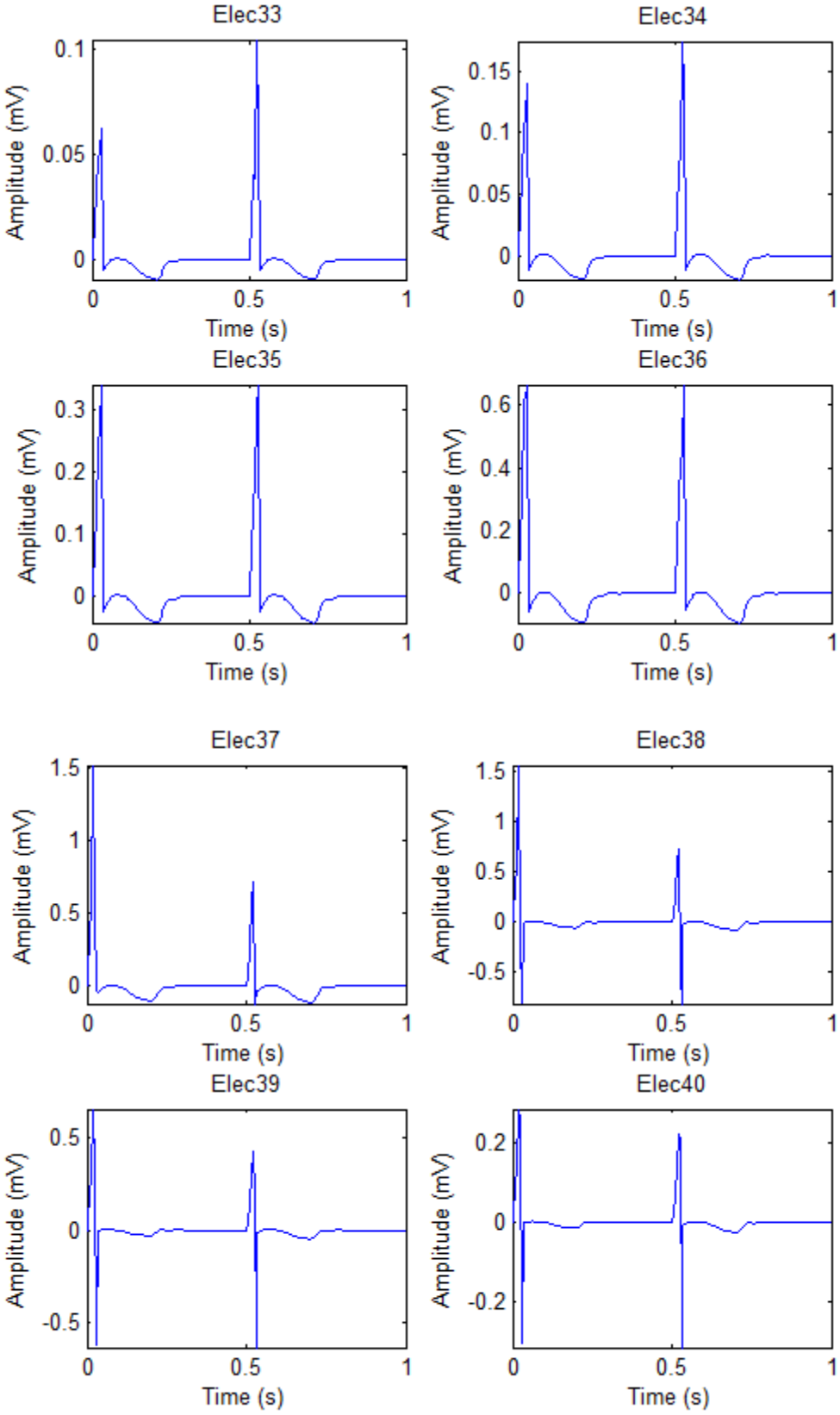
Elec33
Amplitude (mV)
0.1
0.05
0
0
0.5
1
Time (s)
Elec34
Amplitude (mV)
0.15
0.1
0.05
0
0
0.5
1
Time (s)
Elec35
Amplitude (mV)
0.3
0.2
0.1
0
0
0.5
1
Time (s)
Elec36
Amplitude (mV)
0.6
0.4
0.2
0
0
0.5
1
Time (s)
Elec37
Amplitude (mV)
1.5
1
0.5
0
0
0.5
1
Time (s)
Elec38
Amplitude (mV)
1.5
1
0.5
0
-0.5
0
0.5
1
Time (s)
Elec39
Amplitude (mV)
0.5
0
-0.5
0
0.5
1
Time (s)
Elec40
Amplitude (mV)
0.2
0
-0.2
0
0.5
1
Time (s)

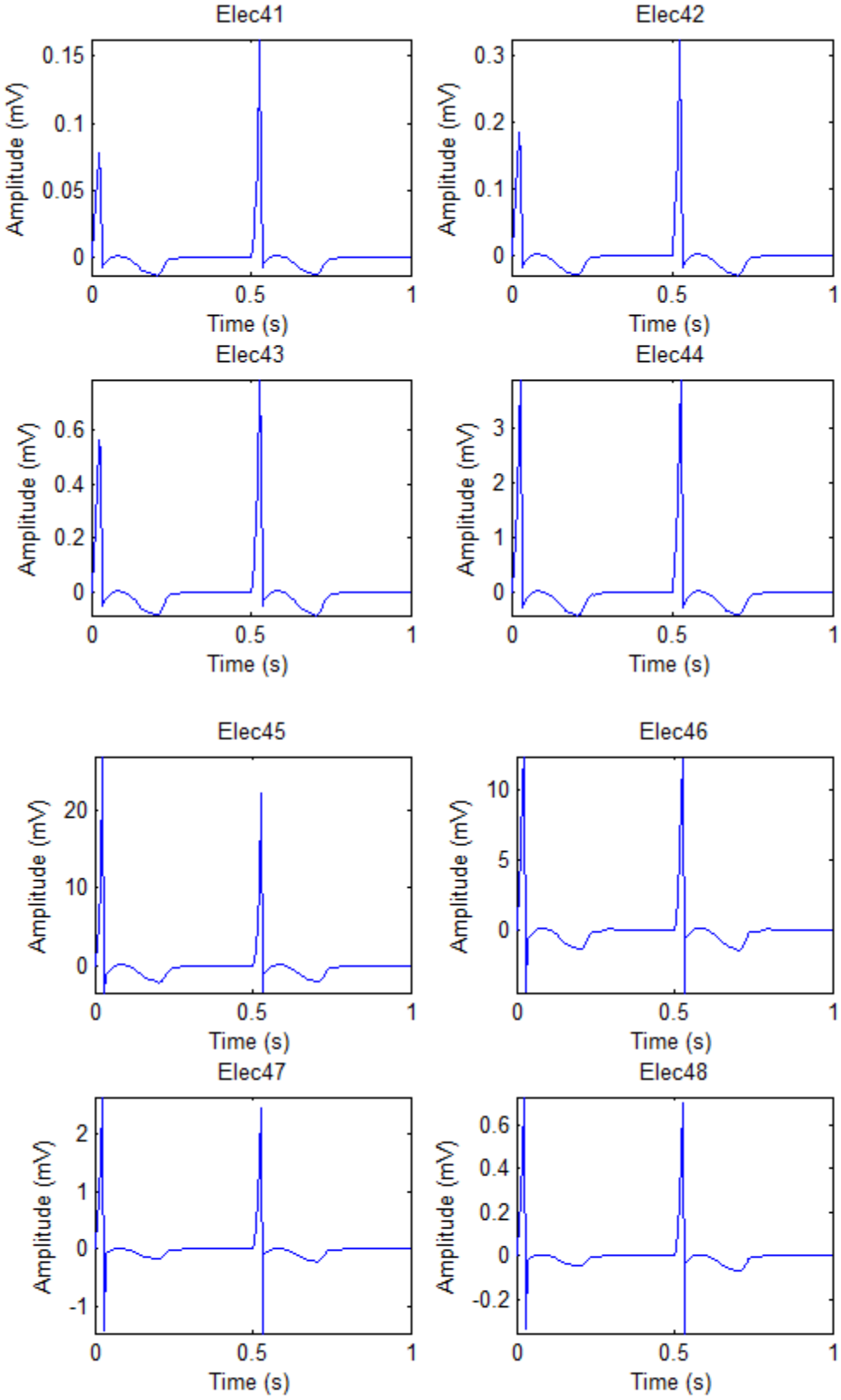
Elec41
Amplitude (mV)
0.15
0.1
0.05
0
0
0.5
1
Time (s)
Elec42
Amplitude (mV)
0.3
0.2
0.1
0
0
0.5
1
Time (s)
Elec43
Amplitude (mV)
0.6
0.4
0.2
0
0
0.5
1
Time (s)
Elec44
Amplitude (mV)
3
2
1
0
0
0.5
1
Time (s)
Elec45
Amplitude (mV)
20
10
0
0
0.5
1
Time (s)
Elec46
Amplitude (mV)
10
5
0
0
0.5
1
Time (s)
Elec47
Amplitude (mV)
2
1
0
-1
0
0.5
1
Time (s)
Elec48
Amplitude (mV)
0.6
0.4
0.2
0
-0.2
0
0.5
1
Time (s)

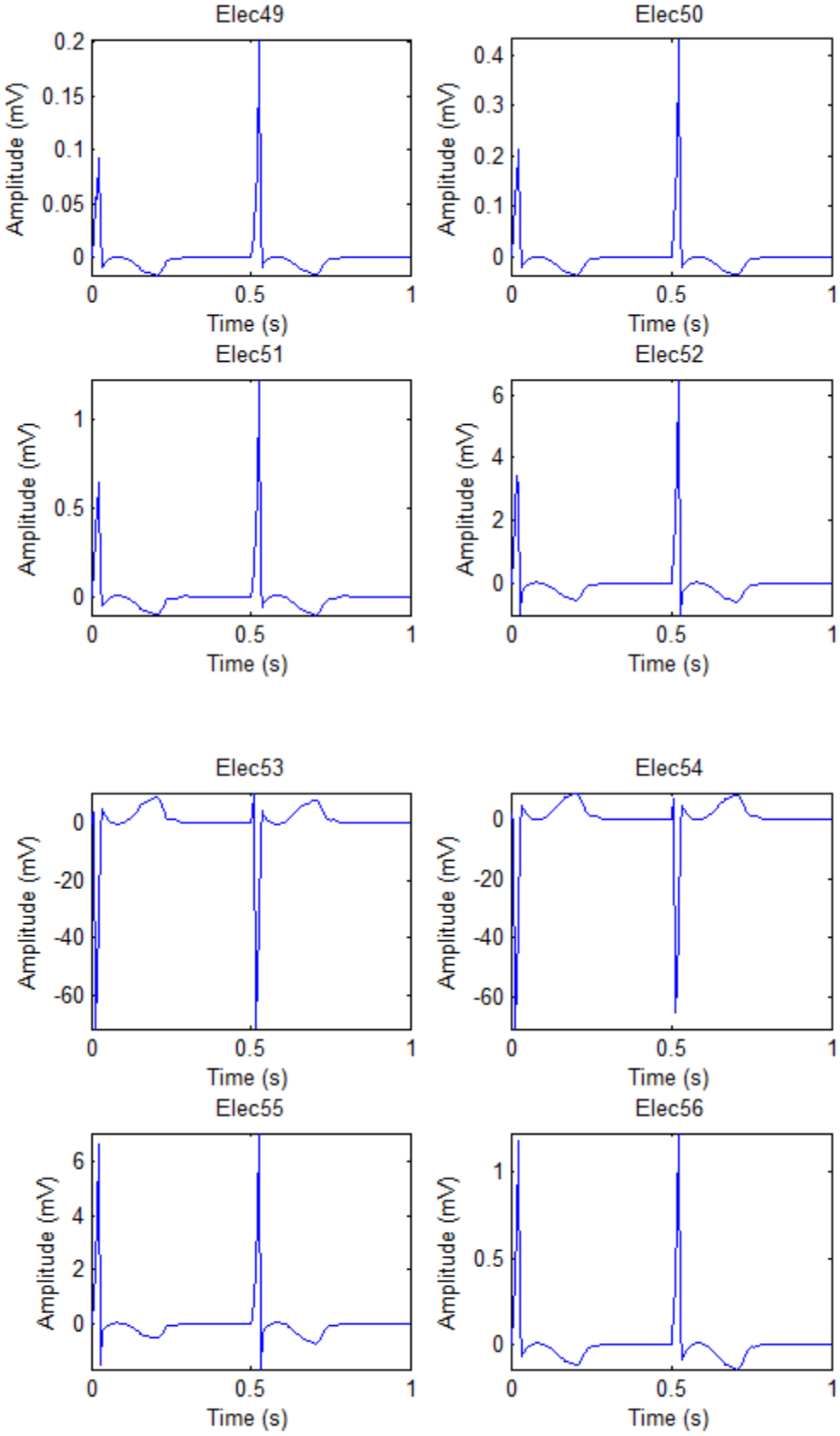
Elec49
Amplitude (mV)
0.2
0.15
0.1
0.05
0
0
0.5
1
Time (s)
Elec50
Amplitude (mV)
0.4
0.3
0.2
0.1
0
0
0.5
1
Time (s)
Elec51
Amplitude (mV)
1
0.5
0
0
0.5
1
Time (s)
Elec52
Amplitude (mV)
6
4
2
0
0
0.5
1
Time (s)
Elec53
Amplitude (mV)
0
-20
-40
-60
0
0.5
1
Time (s)
Elec54
Amplitude (mV)
0
-20
-40
-60
0
0.5
1
Time (s)
Elec55
Amplitude (mV)
6
4
2
0
0
0.5
1
Time (s)
Elec56
Amplitude (mV)
1
0.5
0
0
0.5
1
Time (s)

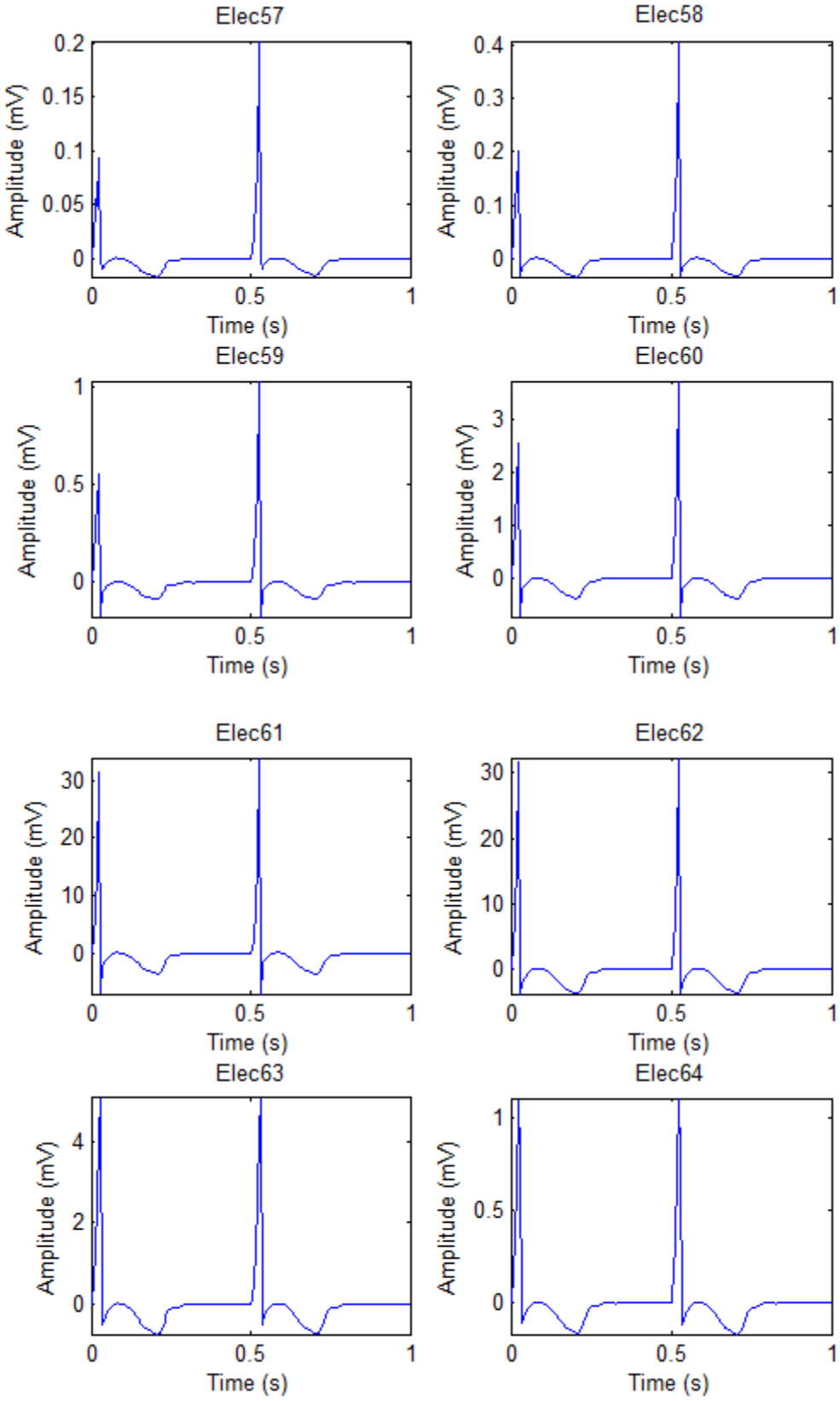
Elec57
Amplitude (mV)
Time (s)
Elec58
Amplitude (mV)
Time (s)
Elec59
Amplitude (mV)
Time (s)
Elec60
Amplitude (mV)
Time (s)
Elec61
Amplitude (mV)
Time (s)
Elec62
Amplitude (mV)
Time (s)
Elec63
Amplitude (mV)
Time (s)
Elec64
Amplitude (mV)
Time (s)